Computational and Structural Biotechnology Reports 1 (2024) 100018

Contents lists available at ScienceDirect

Computational and Structural Biotechnology Reports

journal homepage: www.sciencedirect.com/journal/csbr

Full length article

# Ligand-based pharmacophore modeling, virtual screening, and molecular dynamics simulations of Pfhsp90 fingerprints in *Plasmodium* malaria treatment

Harrison Onyango [a,*], Grace Gitau [b], John Muoma [a], Patrick Okoth [a]

[a] Department of Biological Sciences [Molecular Biology, Computational Biology, and Bioinformatics Section], School of Natural and Applied Sciences, Masinde Muliro University of Science and Technology, Kakamega 190-50100, Kenya
[b] Department of Biochemistry and Biotechnology, School of Biological and Life Sciences, The Technical University of Kenya, Nairobi 52428–00200, Kenya

ARTICLE INFO

*Keywords:*
Malaria
Virtual screening
Molecular dynamics simulation
Pharmacophore
Modeling
Ligand

ABSTRACT

The World Health Organization (WHO) documents malaria as one of the leading causes of high morbidity and mortality worldwide. The disease affects millions and kills thousands of people annually. Efforts to reduce the global burden of malaria have prompted the WHO to recommend prevention strategies such as using antimalarial drugs. However, these strategies have been ineffective because of antimalarial drug resistance. The only efficacious malaria treatment is Artemisinin-based Combination Therapy (ACT). However, the extended ACT clearance times, linked to the emergence of artemisinin monotherapy resistance recorded most recently in Africa and the Great Mekong region, pose a danger to its efficacy. Therefore, better efficacious antimalarial drugs are required. Since P. falciparum heat shock protein 90 (PfHsp90) is a well-characterized malaria drug target, this study uses it to discover more efficacious antimalarial drugs. An in silico approach was used to discover PfHsp90 inhibitors with pharmacological properties against Plasmodium malaria using a molecular dynamics simulation (MDS) and hierarchical virtual screening. Geldanamycin (GDM), a well-known anti-PfHsp90 compound, was used to identify PfHsp90 inhibitors with pharmacological properties against Plasmodium malaria by screening it against the ZINC20 database via the ZINCPHARMER web server. This virtual screening process resulted in 17 hits. These ZINCPHARMER hits were subjected to drug-likeness and pharmacokinetics properties analysis in the SwissADME web server, and nine of them satisfied the requirements. The nine ZINC20 compounds were docked with PfHsp90 using the PyRx software version 0.8 to understand their interactions. From the molecular docking results, ZINC09060002 (−8.2 kcal/mol), ZINC72133064 (−7.8 kcal/mol), ZINC72163401 (−7.7 kcal/mol), ZINC72358537 (−8.1 kcal/mol), and ZINC72358557 (−7.6 kcal/mol) had better binding affinities to PfHsp90 than GDM (−7.5 kcal/mol). The stability of these molecularly docked protein–inhibitor complexes was assessed through MDS using GROMACS 2022. ZINC72163401, ZINC72358537, and ZINC72358557 formed stable complexes with PfHsp90. The lead compounds were subjected to in vitro validation for their inhibitory capability. They showed promising inhibition of parasite growth with IC50 values ranging between 200 and 400 ng/mL. In this regard, the three PfHsp90 inhibitors can be further developed as potential antimalarial drugs. However, further structural optimization studies and clinical (in vivo) tests are necessary to ascertain the antimalarial activity of these compounds in humans.

## 1. Introduction

Malaria is a universal public health burden, with approximately 241 million confirmed cases and approximately 627,000 fatalities in 2020 [1]. These statistics underscore an alarming rise in malaria cases and deaths compared to the WHO's 2019 report. In 2019, the WHO reported 229 million confirmed cases and approximately 409,000 deaths worldwide [2]. Unfortunately, Africa contributes a disproportionally high portion of the global malaria burden, especially sub-Saharan Africa. In 2020, the African region contributed 95 % of malaria-confirmed cases

* Corresponding author.
*E-mail addresses:* harryonyango01@gmail.com (H. Onyango), ggitau@tukenya.ac.ke (G. Gitau), jmuoma@mmust.ac.ke (J. Muoma), okothpatrick@mmust.ac.ke (P. Okoth).

https://doi.org/10.1016/j.csbr.2024.100018
Received 16 August 2024; Received in revised form 21 September 2024; Accepted 27 September 2024
Available online 1 October 2024

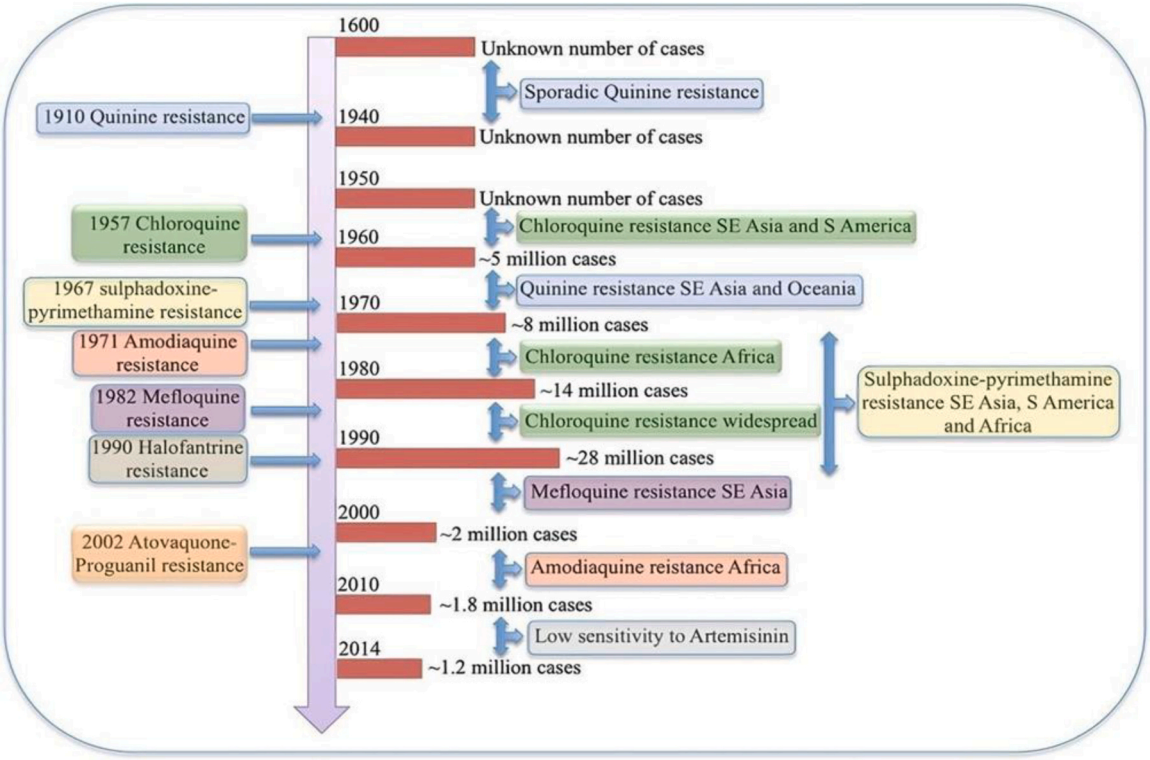


**Fig. 1.** Antimalarial drug resistance. This timeline shows how *P. falciparum* has been mounting resistance to various antimalarial drugs over the years [19].

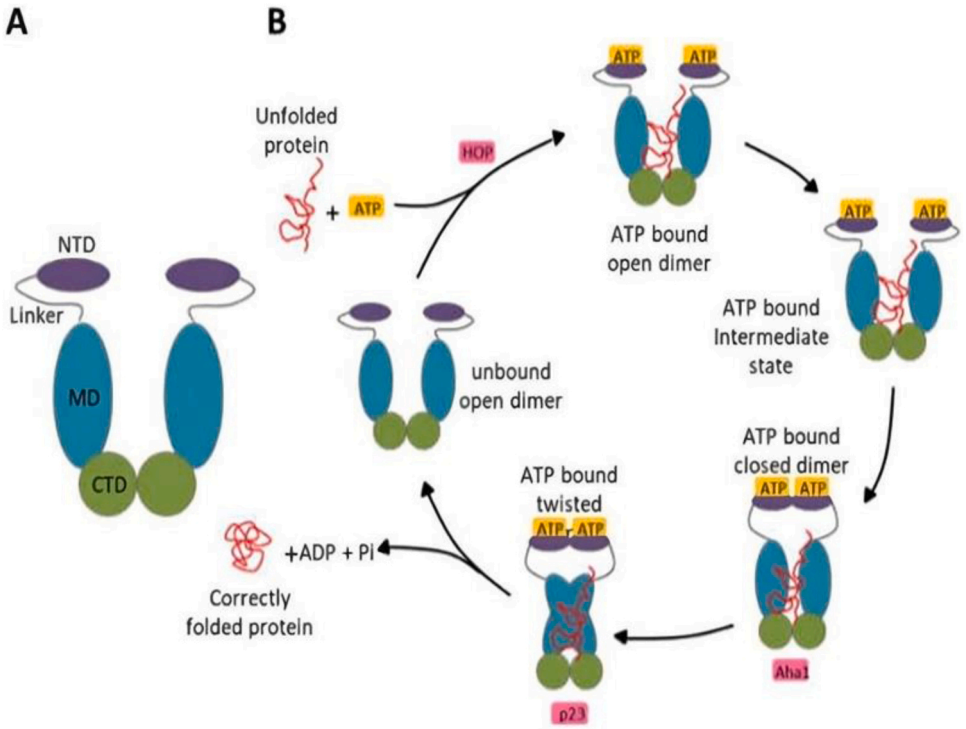


**Fig. 2.** Hsp90 domain organization and functional cycle. (**A**) Schematic representation of the V-shaped domain organization of the Hsp90 protein. (**B**) Schematic representation of the Hsp90 functional cycle begins with the binding of ATP to Hsp90, provoking the association of the protein with a client/unfolded protein. Consequently, a closed conformation is adopted following the NTD dimerization after the lid region of Hsp90 closes over the ATP binding pocket. ATP hydrolysis occurs after repositioning the catalytic loop when the MDs associate. The correctly folded client protein is released upon ATP hydrolysis. This protein folding and ATP hydrolysis cycle reoccurs after the Hsp90 homodimer regains its unbound open configuration and is primed. Aha1, HOP, and p23 are other co-chaperones that modulate this functional cycle [16].

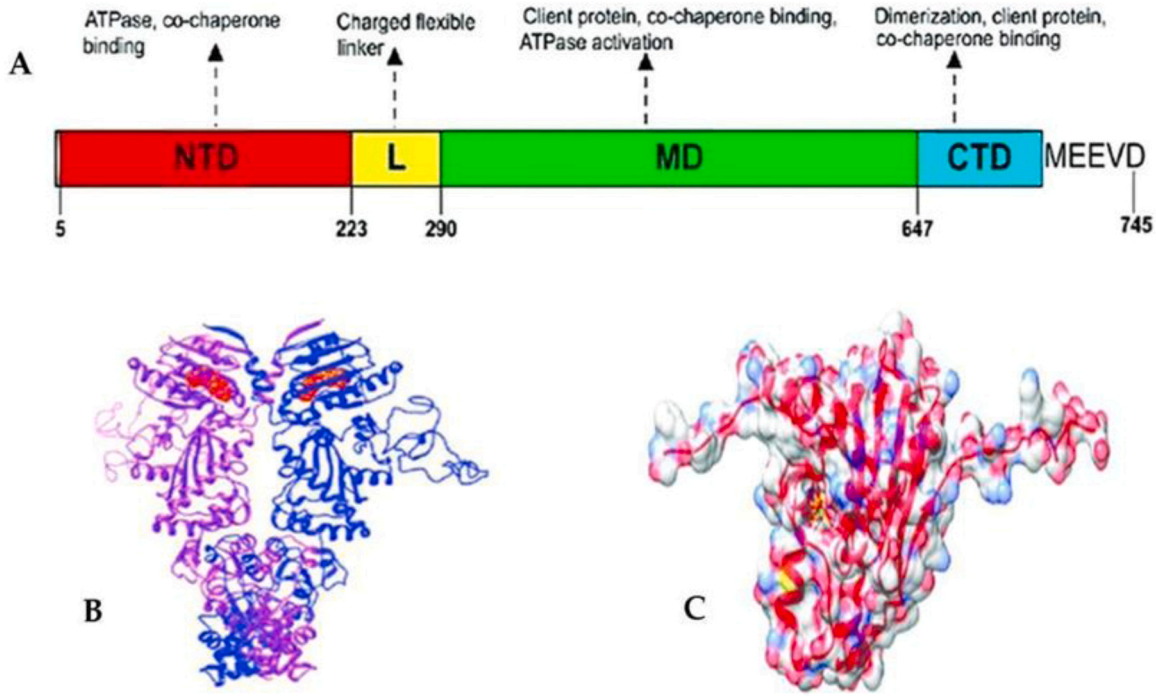


**Fig. 3.** PfHsp90 domain organization and structure view. (**A**) Schematic model of the different PfHsp90 domains labeled NTD (N-Terminal Domain), L (Linker Region), MD (Middle Domain), and CTD (C-Terminal Domain). (**B**) Cartoon representation of PfHsp90 proteins. Red spheres represent ATP bound to NTD. The purple and blue colors in the model depict the two PfHsp90 monomers. (**C**) Surface representation of PfHsp90's NTD with 60 % transparency and colored according to element type [37].

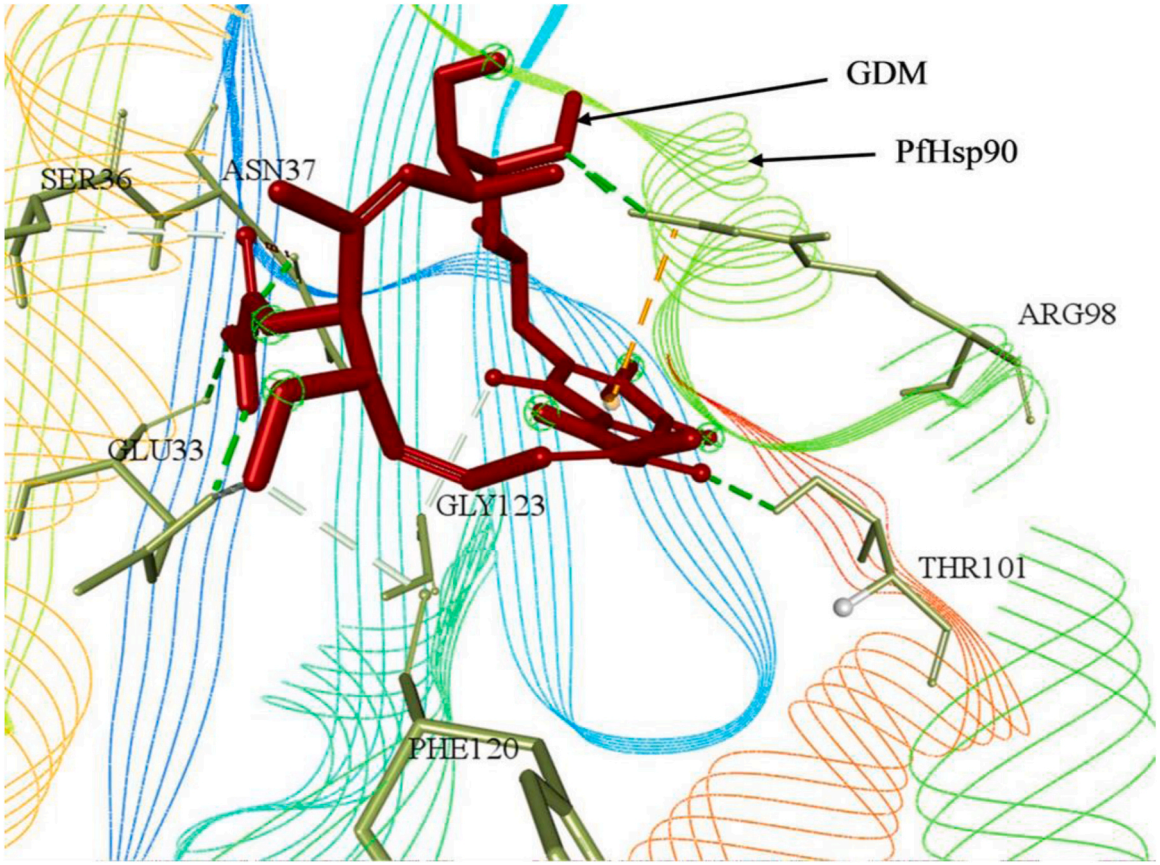


**Fig. 4.** Geldanamycin (GDM) as a PfHsp90 inhibitor. The line ribbon-like structure of different colors is PfHsp90**.** The red stick-like structure represents GDM. The dotted lines display the interaction points between GDM and PfHsp90. BIOVIA Discovery Studio 2021 was used to find the suitable binding pocket pose and show the points of interaction between the two molecules after molecular docking.

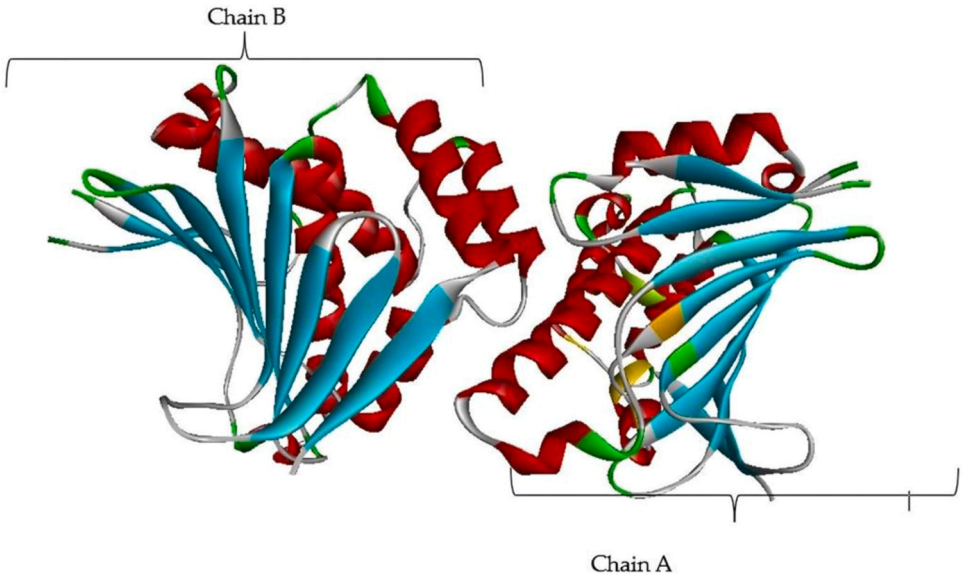


**Fig. 5.** The 3D structure of prepared PfHsp90 NTD. PfHsp90 NTD retrieved from PDB, ID 3K60. All heteroatoms and water molecules removed and polar hydrogens added. The two chains, A and B, are indicated.

**Table 1**
Basic information on GDM.

| Molecule | Name | PubChem CID | Molecular Formular (MF) | Molecular Weight (MW) |
|---|---|---|---|---|
| 1. | Geldanamycin (GDM) | 5288382 | C29H40N2O9 | 560.6 |

and 96 % of malaria deaths [3]. Children aged five years and below accounted for approximately 80 % of all malaria deaths in the African region [3]. Four countries within sub-Saharan Africa accounted for over half of malaria deaths globally [1].

Mosquitoes are the primary vectors of malaria, which primarily affects individuals in subtropical and tropical areas. Obligate protozoan parasites of the genus *Plasmodium* cause the ailment [4]. Mosquito vectors that carry malaria transmit the parasites to people during a blood meal. Once within the host, the parasites first infect the liver cells before moving on to the red blood cells. By altering the infected erythrocytes to make them cytoadherent, malaria parasites cause malaria pathology at the blood stage [5]. Malaria infection, whose incubation period is 7–14 days, can cause lethargy, fatigue, muscle aches, nausea, stomach aches, fever, and shivering [6,7]. Due to the massive loss of red blood cells, the disease can cause jaundice and anemia. Furthermore, if not appropriately treated, malaria can become lethal and cause coma, mental confusion, seizures, kidney failure, and finally, death [8].

To date, *P. falciparum*, *P. knowlesi*, *P. ovale*, *P. vivax*, and *P. malariae* are the five species of *Plasmodium* that can infect individuals and cause malaria. *P. falciparum* has the highest morbidity and fatality rates and hence poses a severe threat to public well-being in locations where malaria is endemic [6,7,9,10]. Currently, malaria kills approximately 400,000 individuals yearly, primarily children in sub-Saharan Africa because they have not yet developed any immunity to the illness. It affects 200–400 million people annually [10–12]. Between 2000 and 2015, antimalarial medications, insecticide-treated mosquito nets, and other public health initiatives helped reduce malaria cases worldwide by 50–75 % [12]. Despite these initiatives, the malaria incidence has grown since 2015 in numerous places for various reasons [12]. One of the outstanding reasons include the parasites developing resistance to

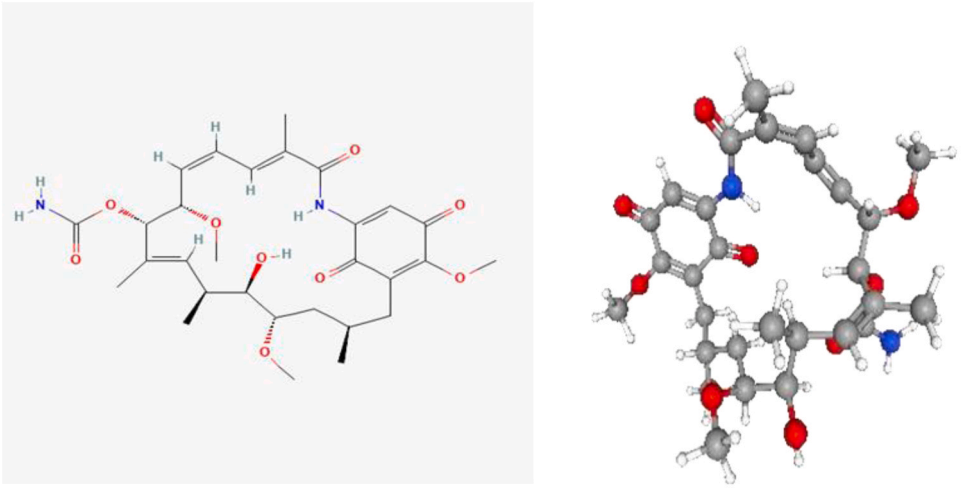

**(A)** **(B)**

**Fig. 6.** 2D and 3D Structures of GDM. (**A**) 2D structure. (**B**) 3D structure.

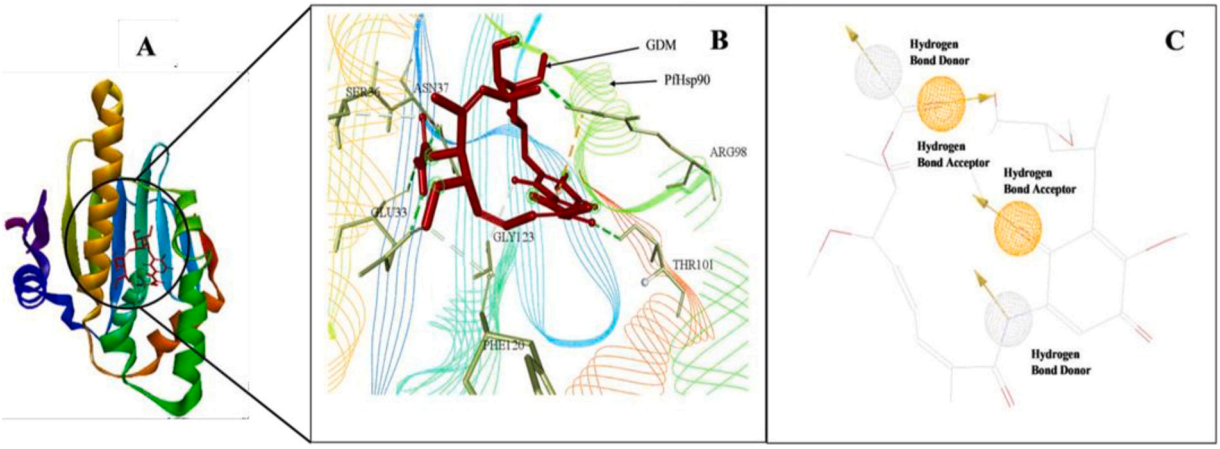


**Fig. 7.** The pharmacophore model created using GDM. (**A**) GDM bound to PfHsp90. (**B**) Interactions between GDM and PfHsp90. (**C**) The four key pharmacophore features in GDM that interacts with key PfHsp90 residues.

**Table 2**
Basic information on the virtual screening results using GDM as ligand.

| No. | Molecule | RMSD | Mass | RBnds |
|---|---|---|---|---|
| 1 | ZINC09060002 | 0.363 | 394 | 4 |
| 2 | ZINC32537723 | 0.380 | 305 | 5 |
| 3 | ZINC92700801 | 0.291 | 296 | 5 |
| 4 | ZINC71617232 | 0.257 | 244 | 6 |
| 5 | ZINC63526364 | 0.342 | 332 | 6 |
| 6 | ZINC71617229 | 0.270 | 244 | 6 |
| 7 | ZINC22325332 | 0.352 | 473 | 7 |
| 8 | ZINC72358557 | 0.332 | 394 | 7 |
| 9 | ZINC72358537 | 0.331 | 410 | 7 |
| 10 | ZINC77271253 | 0.240 | 300 | 7 |
| 11 | ZINC72133064 | 0.279 | 329 | 8 |
| 12 | ZINC72163401 | 0.410 | 315 | 8 |
| 13 | ZINC91416974 | 0.373 | 353 | 8 |
| 14 | ZINC72358880 | 0.330 | 368 | 9 |
| 15 | ZINC32796276 | 0.300 | 453 | 10 |
| 16 | ZINC70981147 | 0.245 | 336 | 15 |
| 17 | ZINC70981147 | 0.249 | 336 | 15 |

antimalarial medicines.

Antimalarial drug resistance, which increases malaria mortality and morbidity, has become a menace that casts doubt on the effectiveness of the currently available antimalarial medications. Only *P. falciparum* and *P. vivax* have been proven to be resistant to the antimalarial drugs currently on the market [13]. *P. knowlesi*, a zoonotic monkey malaria that affects individuals in Southeast Asian forested environments, is completely sensitive to chloroquine and other commonly utilized medications [13]. *P. falciparum* and *P. vivax* are resistant to chloroquine. *P. falciparum* is also resistant to other antimalarial drugs, including quinine, halofrantrine, mefloquine, and sulfadoxine/pyrimethamine [13].

Researchers have argued that Artemisinin-based Combination Therapy (ACT) is the only efficacious malaria treatment [14,15]. However, extended ACT clearance times, which are linked to the emergence of artemisinin monotherapy resistance, have been recorded most recently in Africa and the Great Mekong region and pose a danger to its efficacy [16]. Genotypes of parasites resistant to the artemisinin medication have recently been discovered in Rwanda, indicating extensive artemisinin compound resistance [17]. Molecular chaperones such as Hsps are responsible for the proper folding of mutated chloroquine resistance transporter (CRT) that enhance antimalarial drug resistance.

Due to their crucial function in protein quality regulation, genes, such as the CRT gene linked to multidrug resistance, are situated in the same Hsp90 gene cluster [18]. Hsps' chaperoning function on proteins might facilitate drug resistance during the stress response. Since the 1600 s, attempts have been made to control and manage antimalarial drug resistance in vain [19]. Reported malaria cases have always been in the millions, as displayed in Fig. 1 [19]. Hsp90 can be considered a drug target whose inhibition prevents its role in protein folding and facilitates malaria treatment by reducing the level of antimalarial drug resistance that the parasite can mount within the body.

Hsp90 is an evolutionary conserved and widely expressed molecular chaperones group that accounts for around 2 % of the cellular proteome [20]. Almost all organisms possess Hsp90 proteins, which are necessary

**Table 3**
Drug-likeness test results of the 17 molecules.

| No. | Molecule | Lipinski | Ghose | Veber | Egan | Muegge | Drug-Like? |
|---|---|---|---|---|---|---|---|
| 1 | ZINC09060002 | Yes | Yes | Yes | Yes | Yes | Yes |
| 2 | ZINC32537723 | Yes | Yes | No | No | No | No |
| 3 | ZINC92700801 | Yes | Yes | Yes | Yes | Yes | Yes |
| 4 | ZINC71617232 | Yes | No | Yes | No | Yes | No |
| 5 | ZINC63526364 | Yes | No | Yes | Yes | Yes | Yes |
| 6 | ZINC71617229 | Yes | No | Yes | No | Yes | No |
| 7 | ZINC22325332 | Yes | No | No | No | Yes | No |
| 8 | ZINC72358557 | Yes | Yes | Yes | Yes | Yes | Yes |
| 9 | ZINC72358537 | Yes | No | Yes | Yes | Yes | Yes |
| 10 | ZINC77271253 | Yes | No | Yes | No | Yes | No |
| 11 | ZINC72133064 | Yes | Yes | Yes | Yes | Yes | Yes |
| 12 | ZINC72163401 | Yes | No | Yes | Yes | Yes | Yes |
| 13 | ZINC91416974 | Yes | No | Yes | Yes | Yes | Yes |
| 14 | ZINC72358880 | Yes | Yes | Yes | Yes | Yes | Yes |
| 15 | ZINC32796276 | Yes | Yes | No | No | Yes | No |
| 16 | ZINC70981147 | Yes | No | Yes | Yes | Yes | Yes |
| 17 | ZINC70981147 | Yes | No | Yes | Yes | Yes | Yes |

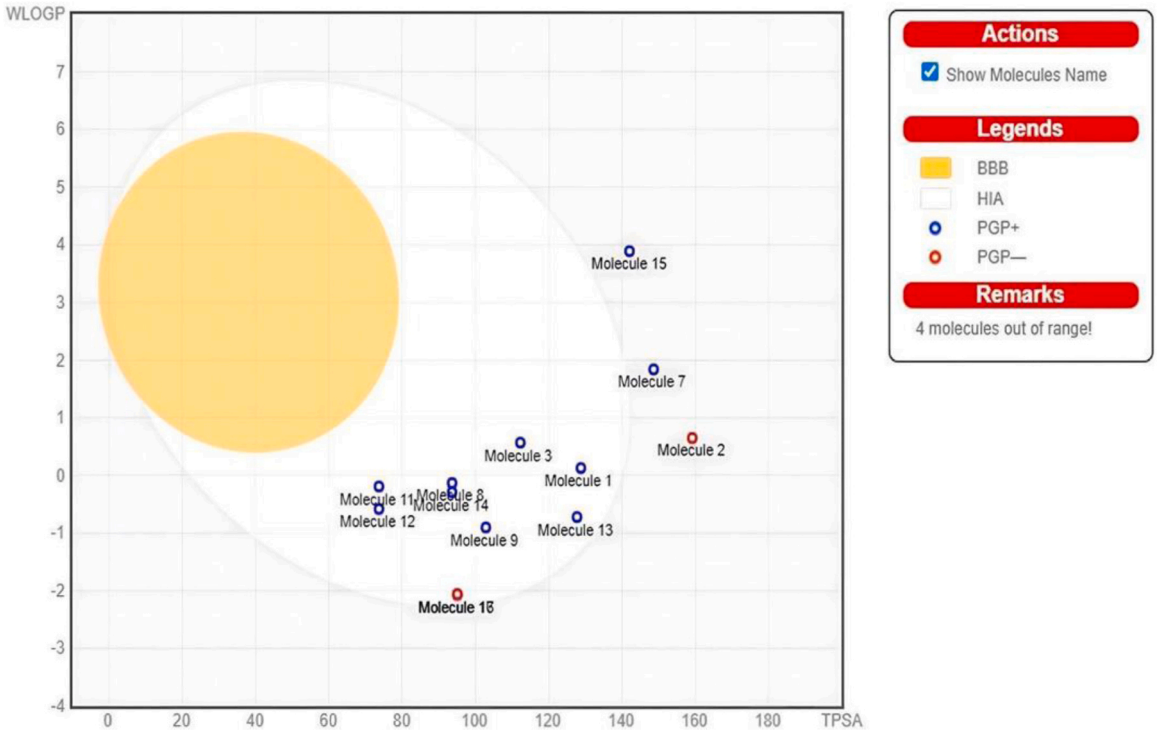


**Fig. 8.** BOILED-Egg Analysis (GDM). Boiled egg prediction of blood–brain barrier permeability and gastrointestinal absorption for the 17 hits. A total of 4 molecules (15, 7, 2, and 16) are out of range, and thus excluded. The other molecules are P-glycoprotein (P-gp) substrate, indicated by the blue dot, depicting their ease of excretion from the body.

for eukaryotes to survive [21,22]. The Hsp90 family members are ATP-dependent chaperones involved in numerous biological functions [22]. Adenosine triphosphate (ATP) binding and subsequent hydrolysis power the Hsp90, which occurs as a V-shaped homodimer functional cycle (Fig. 2) [16]. During this cycle, Hsp90 binds to the ATP-bound state and open-dimer configuration of an unfolded substrate/client protein [23]. The N5, N4, and N1 helixes in the NTD undergo a conformational shift; as a result, they close over the ATP binding pocket and serve as a lid over the cavity [24]. The crucial catalytic residues Gln423, Arg419, and Asn416 that hydrolyze ATP are part of the catalytic loop in P. falciparum, which extends from residues 414 to 427 [25]. The release of the appropriately folded client protein is then made possible by the dissociation of the NTDs brought on by ATP hydrolysis [26,27].

In early studies, Hsp90 inhibitors were primarily used to treat cancer [28]. Hsp90 overexpression in cancerous cells make it a promising target for anti-cancer medications [29]. In *P. falciparum*, Hsp90 proteins are desirable therapeutic targets against *Plasmodium* malaria because they are ATPases with differing activity levels in various organisms [30], and diseased cells have higher ATP hydrolysis rates, making them more vulnerable to ATPase inhibitors [16]. Similarly, *P. falciparum* Hsp90 is more susceptible to inhibition than the human homolog due to its increased ATPase activity [16]. Hsp90 has different co-chaperone interactions that are species-specific enabling selective inhibition [31]. The minor variations in amino acid residues among Hsp90 proteins from various organisms and cellular compartments have also resulted in specific structural variances [32]. Identifying drug targets based on distinctive Hsp90 protein conformations has become easier because of the elucidation of various Hsp90 crystal structures [33]. Numerous crystal structures of various Hsp90 NTDs in complex with inhibitors and nucleotides have been resolved [34]. Additionally, Hsp90's complete structural characterization has prompted the creation of inhibitors targeting its MD [25,31,35] and CTD [36]. Fig. 3 [37] shows PfHsp90's domain organization and structure. Through targeting Hsp90, some inhibitors have been demonstrated to be efficient at reducing the parasite's development [38–40].

One of the first Hsp90 inhibitors discovered was geldanamycin (GDM), a benzoquinone ansamycin molecule naturally generated by Streptomyces hygroscopicus [16]. GDM was initially believed to be an antibiotic that inhibited kinases, but it was later discovered that it had a high degree of selectivity in its binding to Hsp90 [16]. In a study at an IC50 similar to the well-known antimalarial chloroquine (20 nM and 15 nM, respectively), GDM suppressed in vitro parasite development [16]. Fig. 4 shows the interaction between PfHsp90 and GDM.

Several researchers have resorted to the use of in silico means to design and develop drugs, shying away from the traditional techniques that are expensive and time-consuming. Some of the most common computational methods used in drug design and discovery include drug design visualization, hierarchical virtual screening, molecular dynamics simulations, and molecular docking [41]. These in silico methods have been applied by numerous researchers to create drug candidates. For instance, in silico techniques have been used to identify prospective anti-SARS-CoV-2 main protease (Mpro) medicines [42]. Similarly, 15 effective anti-viral Mpro compounds have been discovered using in silico methods, including chloroquine, cilexetil, dipyridamole, hydroxychloroquine, and candesartan [43].

In silico methods have been used to ascertain that the synthetic derivatives of 1-(heteroaryl)−2-((5-nitroheteroaryl) methylene) hydrazine that showed anti-plasmodial activities in vitro also possessed the same capability in vivo [44]. In a similar study, in silico approaches were utilized to assess the capability of repurposing approved antimalarial medicines against COVID-19 [45]. These studies prove that in silico methodologies are ideal during the first phase of the drug development process, discovery and development, and can complement the next two phases, preclinical and clinical research.

After discovering potential drug candidates using computational means, undertaking further in vitro and in vivo validation of their therapeutic capacity is essential. In most cases, the in vitro drug sensitivity assays are utilized depending on the illness and pathogen of interest. In a systematic review, various drug sensitivity assays utilized for antimalarial drug efficacy testing targeting different stages of the

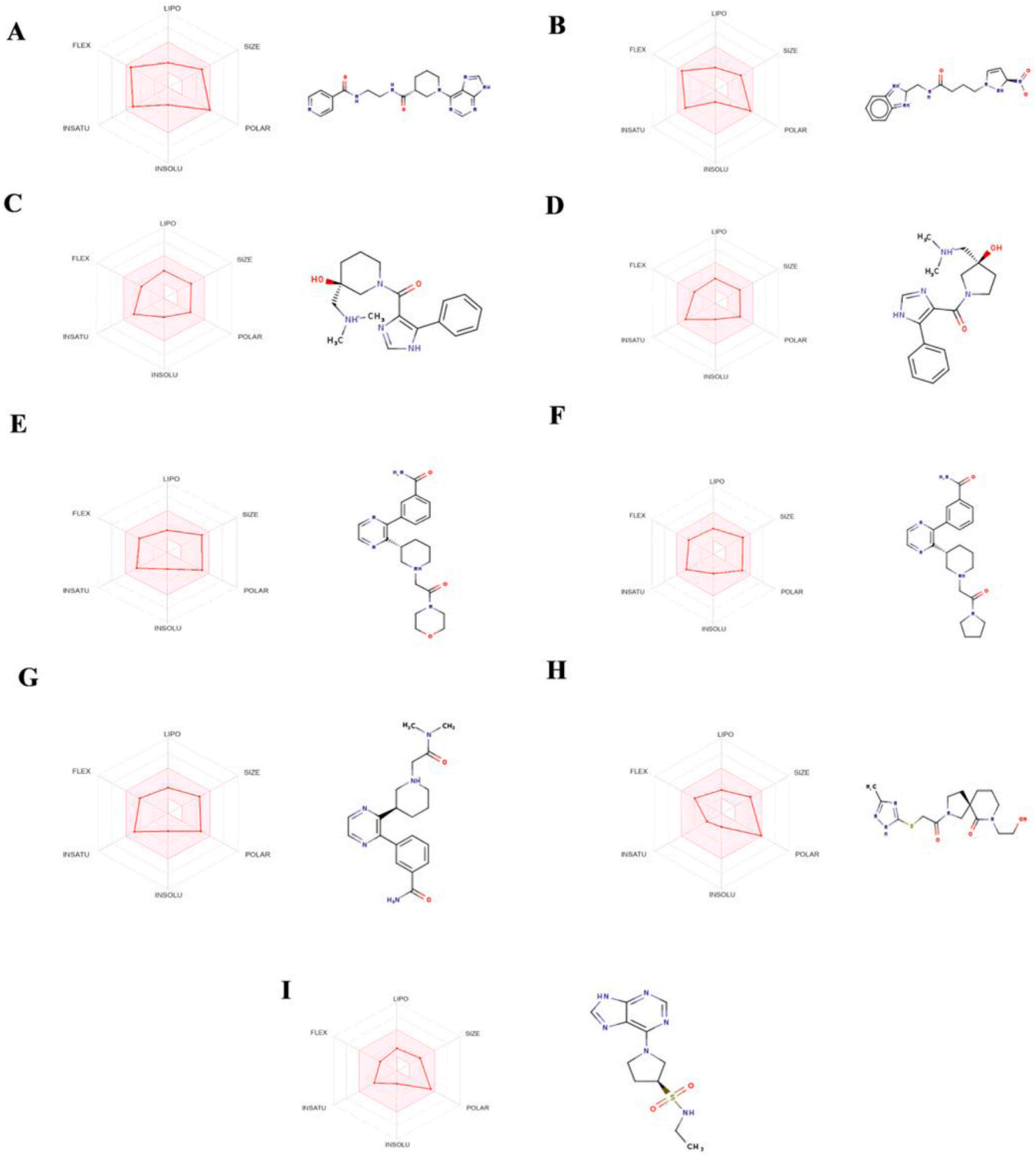


**Fig. 9.** The structures and oral bioavailability radars of the 9 Hits. (**A**) ZINC09060002, (**B**) ZINC63526364, (**C**) ZINC72133064, (**D**) ZINC72163401, (**E**) ZINC72358537, (**F**) ZINC72358557, (**G**) ZINC72358880, (**H**) ZINC91416974, (**I**) ZINC92700801.

parasite's development were pointed out [46]. Some of those assays include blood stages assays (Schizont maturation, microscopic assay, radioisotopic assays, and enzymatic assays), gametocytes stage assays (oxido-reduction indicator, Alamar blue, and SMFA), liver stage assays (infrared fluorescence detection method), and HTS (fluorescence-based assay and in vitro beta-hematin formation assay) [46].

One of the most common antimalarial drug sensitivity assays is the SYBR green assay. It is considered the gold standard for in vitro malaria drug sensitivity testing because of its reliability as a drug screening and surveillance tool [47]. It is also described as a simple and cost-effective methodology that has been utilized to determine the 50 % inhibitory concentrations (IC50) of clinical isolates [47]. Researchers have used this assay in their studies, including when assessing the susceptibility of *P. falciparum* isolates to antimalarial medicines in Mali [48]. Similarly, the susceptibility of *P. falciparum* isolates to 11 antimalarial medicines using the SYBR green assay have been assessed [49]. The antimalarial

**Table 4**
Binding affinities of GDM and the nine lead compounds to PfHsp90.

| No. | Molecule | Binding Energy (kcal/mol) |
|---|---|---|
| 1 | GDM | −7.5 |
| 2 | ZINC72163401 | −7.7 |
| 3 | ZINC72133064 | −7.8 |
| 4 | ZINC09060002 | −8.2 |
| 5 | ZINC72358557 | −7.6 |
| 6 | ZINC72358537 | −8.1 |
| 7 | ZINC92700801 | −6.7 |
| 8 | ZINC63526364 | −7.1 |
| 9 | ZINC91416974 | −7.0 |
| 10 | ZINC72358880 | −7.1 |

drugs included PND, lumefantrine (LMF), quinine (QN), artemether (AM), DHA, artesunate (AS), pyrimethamine (PY), NQ, mefloquine (MFQ), PPQ, and chloroquine (CQ) [49]. Therefore, this assay determined the inhibitory capability of the selected PfHsp90 inhibitors.

## 2. Results

### 2.1. PfHsp90 structure retrieval and preparation

The 3D structure of the NTD of PfHsp90 was retrieved from the PDB database using PDB ID 3K60. It was loaded into BDS 2021 and prepared for molecular docking. It was discovered that the NTD of PfHsp90 contains two chains, A and B, as shown in Fig. 5. Several active sites of the NTD were within chain A. Therefore, during preparation, chain B was deleted, leaving behind a prepared chain A of PfHsp90 NTD, also presented in Fig. 5.

### 2.2. Retrieval of geldanamycin (GDM) structures

From the PubChem library database, the 2D and 3D structures of GDM were retrieved. The molecular weight, molecular formular, and PubChem CID of the compound were collected. This information is summarized in Table 1 and Fig. 6.

### 2.3. Pharmacophore-based virtual screening

The 3D structure of GDM was loaded into the ZINCPHARMER web server. Four of GDM's features, namely, two hydrogen donors (interacting with GLU 33 and ASN 37 and one freely available) and two hydrogen acceptors (interacting with SER 36 and GLY 123) that are integral in the interaction between GDM and PfHsp90 were selected to act as the preferred pharmacophore features. The pharmacophore model created is displayed in Fig. 7. The pharmacophore model was validated via superimposition as evident in Fig. 7C. The virtual screening process was then initiated, resulting in 17 hits (Table 2). The 17 hits were downloaded and saved in a.sdf file.

### 2.4. Drug-likeness and pharmacokinetics test

The hits were then subjected to a drug-likeness test and pharmacokinetics analysis using the SwissADME web server (http://www.swissadme.ch/ (accessed on 15 October 2023)). The drug-likeness test

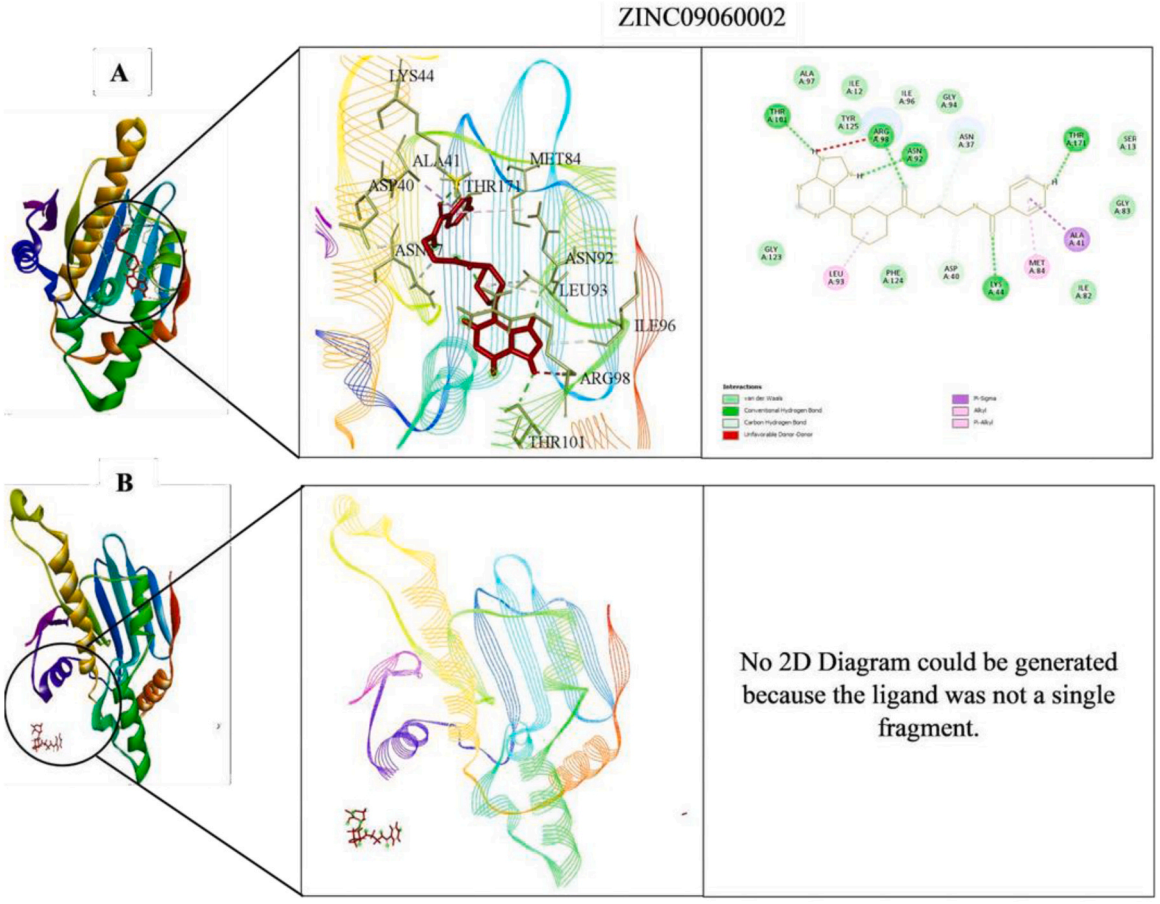


**Fig. 10. .** (**A**) 3D and 2D Interactions of PfHsp90 and the six ligands after molecular docking (at 0 ns). PfHsp90 and ZINC09060002, with binding affinity of −8.2 kcal/mol. PfHsp90 and ZINC72133064, with binding affinity of −7.8 kcal/mol. PfHsp90 and ZINC72163401, with binding affinity of −7.7 kcal/mol. PfHsp90 and ZINC72358537, with binding affinity of −8.1 kcal/mol. PfHsp90 and ZINC72358557, with binding affinity of −7.6 kcal/mol. PfHsp90 and GDM, with binding affinity of −7.5 kcal/mol. (**B**) 3D and 2D Interactions of PfHsp90 and the six ligands after 100 ns molecular dynamics simulation.,.

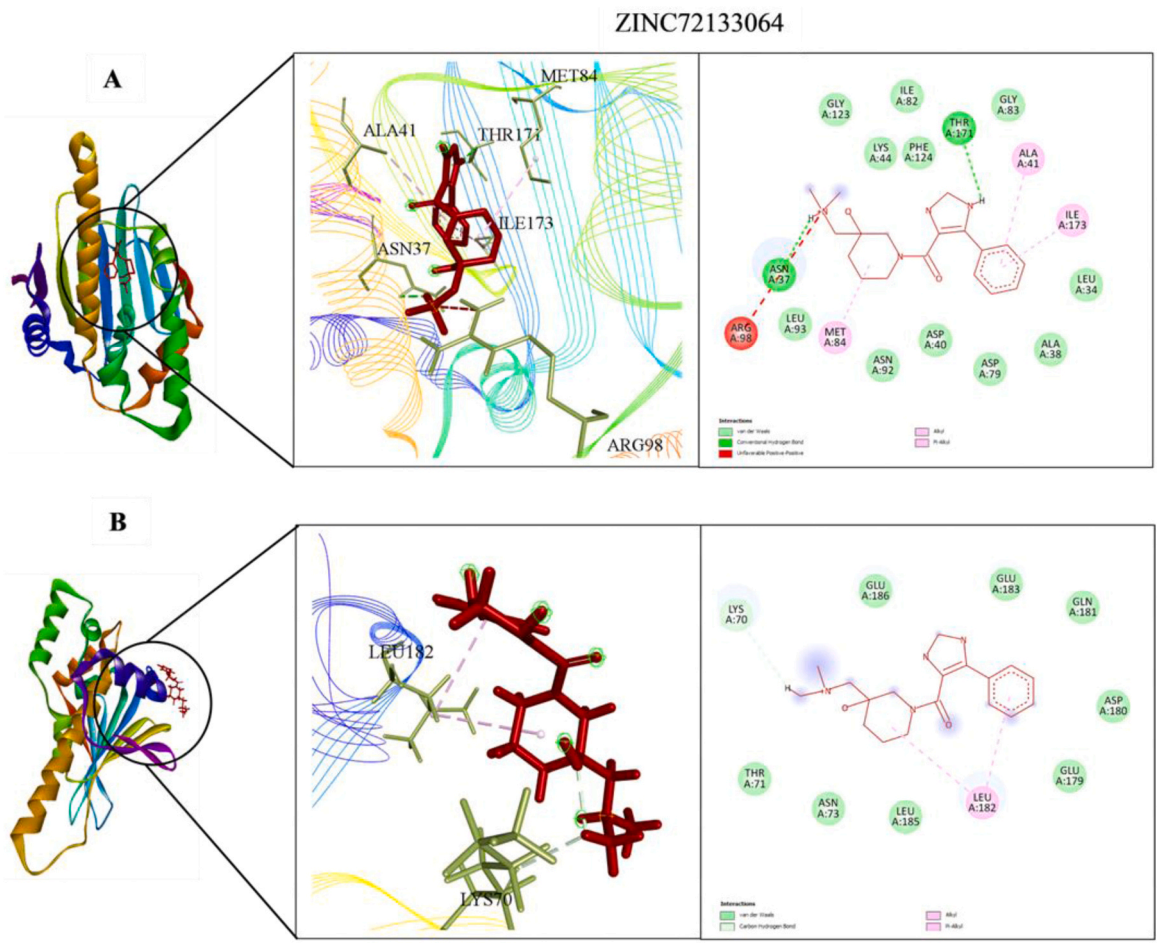


**Fig. 10.** (*continued*).

results are as displayed in Table 3. All the 17 hits were not Pan Assay Interference Structures (PAINS), evident from the SwissADME results that showed 0 alerts. Eleven of the seventeen hits satisfied at least four of the five drug-likeness filters. Therefore, they were selected for further pharmacokinetics analysis. Three other hits were excluded because of their unfavorable pharmacokinetics properties as evident in Fig. 8. Nine hits (Fig. 9) were selected for docking studies.

### 2.5. Molecular docking

The prepared PfHsp90 (PDB ID 3K60) was loaded into the PYRX software version 0.8 as a.pdb file and converted into a.pdbqt molecule for docking purposes. A file containing GDM and the nine lead compounds in the.sdf format was then loaded into the PYRX software version 0.8. The energy of all 10 ligands was minimized. The ligands were then converted into the preferred.pdbqt format. Docking was then performed. As a docking validation process, adenosine diphosphate (ADP), the co-crystallized inhibitor, was re-docked to the NTD of PfHsp90 using PyRx version 0.8. The superimposition of the best pose of the PfHsp90-ADP complex on the docking pose found during crystallization proved the similarity between the two poses as evident in the Supplementary Figures (Fig. S1, Fig. S2, and Fig. S3), suggesting that the docking method used was accurate. The energy range obtained after docking was low, 2.5 kcal/mol, suggesting that the docking process was consistent, reliable, and of high quality. The results confirmed that only five ligands had better binding affinities than GDM. The binding affinities of GDM and the other potential PfHsp90 inhibitors to PfHsp90 are summarized in Table 4. Molecules 2 to 6 had better binding affinities to PfHsp90 than GDM. The other four molecules, 7–10, had lower binding affinities to PfHsp90 than GDM. Therefore, the five ligands with better binding affinities than GDM were considered for molecular dynamics simulation. Fig. 10 A shows the interaction between PfHsp90 and the six ligands.

### 2.6. Molecular dynamics simulation (MDS)

The docked complexes were loaded into the CHARMM-GUI web server as.pdb files to obtain the topology and parameter files. The files were then used to run minimization, equilibration, and production steps of MDS in GROMACS 2022. After the final 100 ns run, the production step, the 2D and 3D molecular interactions between PfHsp90 and the six ligands, were visualized in BIOVIA Discovery Studio (Fig. 10B). These molecular interactions at 100 ns were compared with the initial interactions at 0 ns (after molecular docking) to determine whether there were any similar interactions or loss of interactions (Fig. 10 A,B). ZINC09060002 and ZINC72358537 lost their interactions with PfHsp90. Although ZINC72133064, ZINC72163401, ZINC72358557, and GDM lost some of their interactions, they also created others that enabled them to maintain their binding within PfHsp90's binding pocket.

Similarly, the root-mean-square deviation (RMSD), root-mean-square fluctuation (RMSF), and hydrogen bonds analysis was performed. As shown in Fig. 11, three (ZINC72163401, ZINC72358537, and ZINC72358557) of the five ZINC20 database compounds did not experience major deviations. The conformational change in their backbone atoms in complex with PfHsp90 is comparable to the conformations of GDM in complex with the target protein over 100 ns MDS. ZINC72163401 and ZINC72358557 had a negligible deviation distance of approximately 0.3 nm within PfHsp90's binding pocket throughout the 100 ns MDS. These results confirmed that ZINC72163401 and

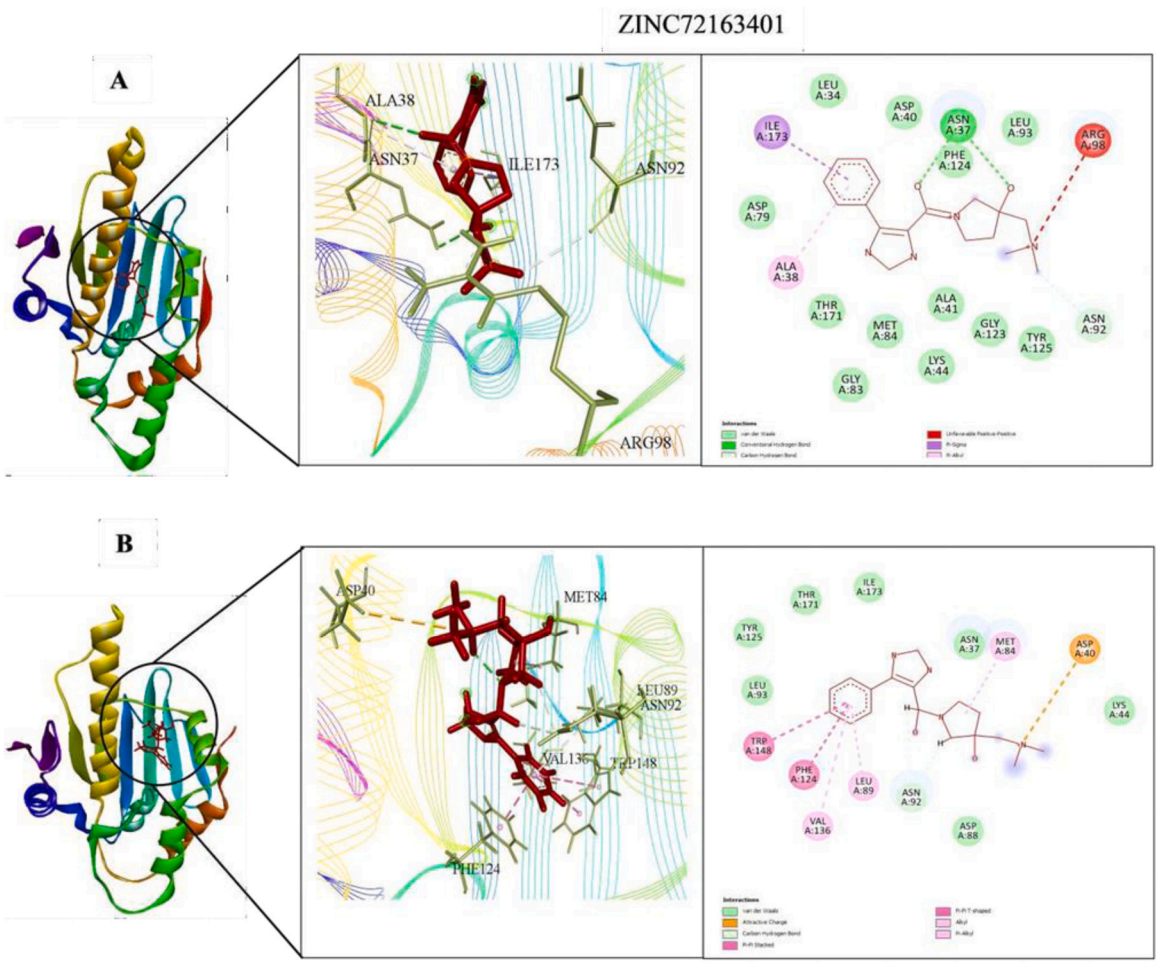


**Fig. 10.** (*continued*).

ZINC72358557 were tightly bound in PfHsp90's active site and could not affect the overall topology of the target protein because their RMSD values were comparable to that of the reference structure (GDM). From Fig. 10, it is evident that the RMSD value of GDM was within 0.25 to 0.75 nm. ZINC72163401 and ZINC72358557 also had RMSD values within that same range. The low RMSD values indicate that the two compounds have stable conformations when complexed with PfHsp90. As for ZINC72358537, before 25 ns and after 85 ns, its deviation distance was almost 4 nm. The deviation distance was below 0.25 nm between 25 ns and 85 ns. Nonetheless, when compared to the RMSD value of GDM, ZINC72358537 had very high RMSD values that ranged between 0.25 to 5.5 nm. ZINC09060002 and ZINC72133064 had high RMSD values throughout the 100 ns MDS, indicating an increased risk of conformational changes in complex with PfHsp90.

The RMSF was calculated to indicate the individual residue flexibility, or how much a specific residue moved (fluctuates) during the 100 ns simulation. It is a structural indication of which amino acids in a protein or atoms in a chemical compound contribute the most to a molecular motion. In the process, the RMSF measures the movement of a specific atom, or group of atoms, in relation to the reference structure, averaged over the number of atoms [50]. Fig. 12 shows the RMSF values of the five ZINC20 database compounds. The GDM fluctuated within a distance of 0.175 nm, with the residue at around position 3450, attaining the lowest fluctuation of approximately 0.025 nm and the atom at position 3505 reaching a maximum fluctuation of almost 0.2 nm. ZINC72358537 and ZINC72163401 also fluctuated within this range, indicating low divergence from the average position and therefore low structural mobility. Even though ZINC72358557 and ZINC72133064 had atoms that attained a lowest fluctuation of 0.025 nm, similar to GDM, some of their atoms surpassed the maximum fluctuation threshold of 0.2 nm to approximately 0.25 nm. Regardless, this 0.05 nm difference is low, making them within the desired RMSF levels. As for ZINC09060002, its highest fluctuation surpassed 0.4 nm, indicating an increased risk of high divergence from the average position and therefore high structural mobility when compared to GDM. These results confirmed that ZINC72163401, ZINC72358537, ZINC72133064, and ZINC72358557 did not undergo high divergence from the average positions.

Hydrogen bonds are essential in protein–ligand complexes because they are considered facilitators of protein–ligand binding. They are believed to increase the affinity with which a ligand binds to a target protein. Fig. 13 shows the number of bonds between PfHsp90 and the six ligands. As the reference, PfHsp90-GDM complex forms 1–3 hydrogen bonds in the course of the 100 ns simulation. ZINC09060002 formed a maximum of four hydrogen bonds with PfHsp90, ZINC72133064 formed three, ZINC72163401 formed four, ZINC72358537 formed four, and ZINC72358557 formed six. These results confirmed that all the five ZINC20 database compounds bind strongly to PfHsp90 when compared with GDM.

### 2.7. *In vitro validation of PfHsp90 inhibitors*

The in vitro activities of PfHsp90 inhibitors and chloroquine as the reference drug were analyzed against field isolates of the parasite, *P. falciparum*. Fig. 14 shows promising inhibition of parasite growth, with IC50 values of 271.54 ng/mL (ZINC72163401), 384.70 ng/mL

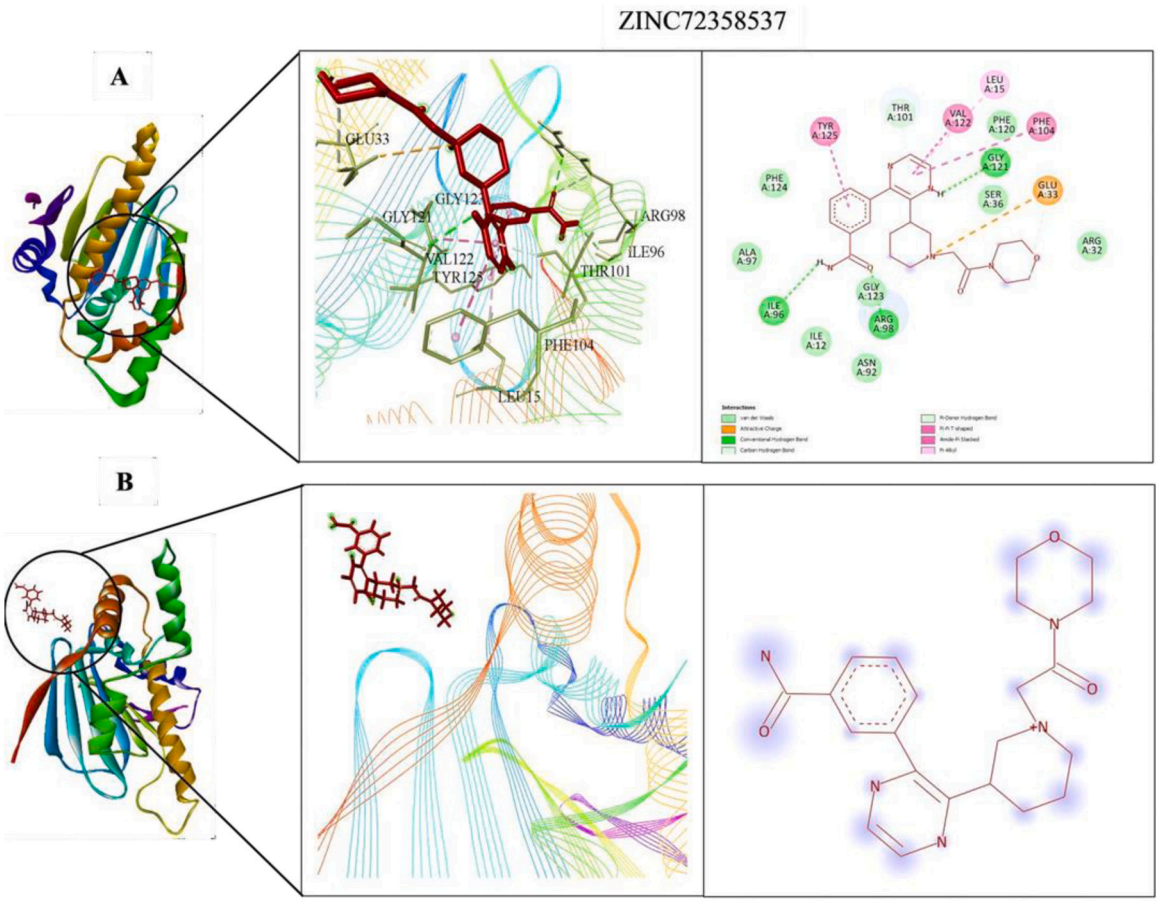


**Fig. 10.** (*continued*).

(ZINC72358537), 241.66 ng/mL (ZINC72358557), and 206.47 ng/mL (Chloroquine). When converted to nM, these IC50 values were 86.86 nM (ZINC72163401), 123.06 nM (ZINC72358537), 77.30 nM (ZINC72358557), and 66.05 nM (chloroquine).

## 3. Discussion

While several licensed treatment regimens exist, malaria still causes a considerable number of fatalities because of its antimalarial drug resistance, heightening the need for novel chemotherapeutic interventions [51,52]. Targeting a distinct parasitic pathway that differs significantly from the host's is a valuable means to prevent the spread of the malarial parasite. Since PfHsp90 facilitates parasite growth during its asexual blood phase [38], *Plasmodium falciparum* uses it to cause malaria. In this regard, inhibiting this protein may hold promise for a *Plasmodium falciparum* malaria cure.

Currently, there is a paradigm shift from traditional to computational approaches of novel drug design and discovery. In silico approaches are gaining traction as options for drug discovery. Numerous studies have used in silico approaches in the discovery of novel therapeutic compounds against malaria, which have progressed to clinical trials [53,54]. *P. falciparum* dihydroorotate dehydrogenase (PfDHODH) inhibitor (DSM265) has been reported to possess antimalarial activity, which has progressed through phase 2 of clinical trials [55–58].

Z1481646084, Z24317941, and Z951873618 were discovered as potential antimalarial compounds inhibiting PfDHODH using in silico means without subjecting them to in vitro and in vivo validation [55]. Now that the use of in silico methods to find novel antimalarial compounds is limited, and the existing in silico studies focus mainly on *P. falciparum* DHODH and no other parasite enzymes or proteins like PfHsp90, there is a need to widen the scope of antimalarial drugs discovery. This study sought to discover PfHsp90 inhibitors as antimalarial drugs.

A virtual screening process was performed using GDM as the ligand to identify the best scoring natural compounds with the ability to inhibit PfHsp90. Due to GDM's vast stereochemical properties that could limit the number of ZINCPHARMER hits obtained, a pharmacophore model was developed using some of its pharmacophore features. These features often interact with key residues within the binding pocket of the target protein of interest, in this case, the NTD of PfHsp90. A few existing studies have identified these key residues. For instance, ASN 37 was identified as one of the essential amino acid residues for ATP binding [59]. It has a side chain oxygen that accepts hydrogens during binding; hence, its interaction with one of GDM's hydrogen donors was selected as a pharmacophore feature in this current study. Even though the focus was on assessing the binding of a specific peptide to the NTD of Hsp90, the authors discovered that the interactions are comparable to those made by GDM [59]. The authors identified Thr174, Asp82, Gly86, Lys47, Gly125, Glu36, and Asp43 as some of the key amino acid residues involved in the interaction [59]. Some of these key residues are in close proximity to GLU 33 and GLY 123, which were used in this study to create the pharmacophore model.

Pharmacophore-based virtual screening, which necessitates the development of a pharmacophore model, is a common in silico approach used today by several researchers [60,61]. The pharmacophore-based virtual screening in this study yielded 17 hits (Table 2). All the ZINCPHARMER hits were subjected to other in silico processes because of their low RMSD values (below 1 Å), which suggests that all the hits are structurally similar to GDM. Other scholars have performed pharmacophore-based virtual screening and focused on RMSD values of

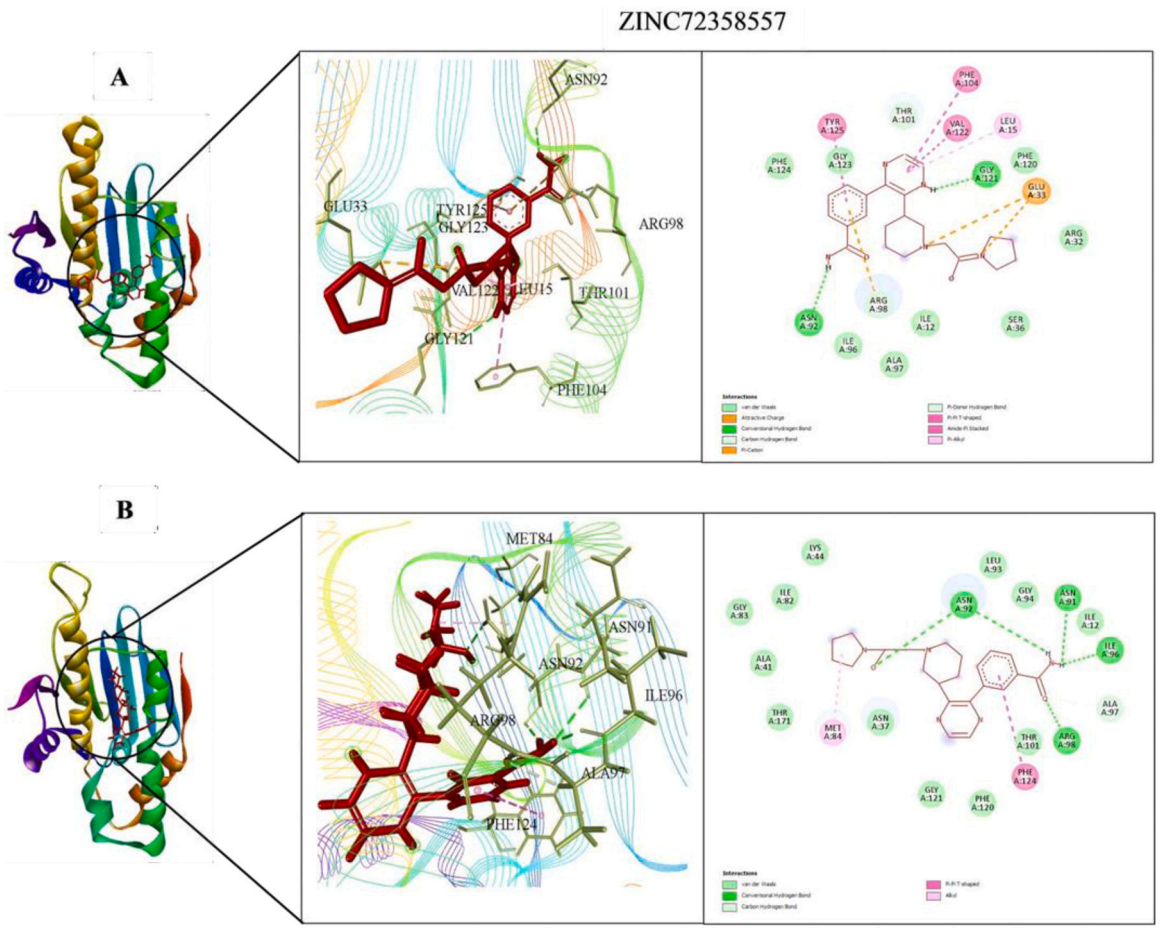


**Fig. 10.** (*continued*).

their hits to determine the most suitable inhibitors against different *P. falciparum* proteins [55,62]. Usually, more similar compounds or proteins have small RMSD values [62]. Therefore, the RMSD values below 1 Å found in this current study suggest the suitability of all the ZINCPHARMER hits as potential PfHsp90 inhibitors. However, this is subject to confirmation via other in silico processes such as a drug-likeness test, ADMET property analysis, molecular docking, and MDS.

Even though several studies performed molecular docking of lead compounds to target proteins before drug-likeness and ADMET property analysis [42,55,62,63], drug-likeness and ADMET property analysis were performed before molecular docking to remove all lead compounds with unsuitable drug characteristics. This approach is consistent with other studies [42,62]. The drug-likeness test and ADMET properties analysis yielded nine potential PfHsp90 inhibitors with drug-likeness and ADMET characteristics for further molecular docking (Fig. 9).

After determining the nine potential PfHsp90 inhibitors, our intent to determine the stability of the complexes they form with PfHsp90 necessitated two in silico process, molecular docking and MDS. These two in silico approaches are common in drug design and discovery [41]. Regarding the binding affinity of GDM to PfHsp90 (−7.5 kcal/mol), only five of the nine PfHsp90 inhibitors had better binding affinities: ZINC72163401 (−7.7 kcal/mol), ZINC72133064 (−7.8 kcal/mol), ZINC09060002 (−8.2 kcal/mol), ZINC72358557 (−7.6 kcal/mol), and ZINC72358537 (−8.1 kcal/mol) (Fig. 10). This means that five of the PfHsp90 inhibitors could bind more strongly to PfHsp90 than GDM.

Despite the positive results of the molecular docking, which validated this study's design rationale, additional MDS studies were performed to confirm and validate the stability of PfHsp90–ligand complexes. To identify, analyze, and provide insights for future lead optimization, six molecular dynamic simulation tests were performed. The stability of the ligand when complexed with PfHsp90 and its binding pocket was shown by the ligands RMSD analysis. The RMSD was used to evaluate the structural changes of the six PfHsp90–ligand complexes. In this study, a stable ligand–protein interaction was indicated by the plot of ligand RMSD vs. time (100 ns), which was within the average limits. This finding was true for all the lead compounds except ZINC09060002 and ZINC72133064, which did not demonstrate the required stability, evidenced by the high RMSD values reaching 4 nm (Fig. 11).

ZINC72163401, ZINC72358537, and ZINC72358557 had average RMSD values of 0.25 nm, suggesting that the conformation of the complex formed between these candidate drugs and PfHsp90 remained relatively stable throughout the 100 ns simulation. Usually, low RMSD values regarding the true binding pose between a ligand and target protein suggest the low binding energy or high binding affinity that facilitates stability [64]. Some studies conclude that protein–ligand complexes that deviate at distances between 1.5 and 4.0 Å, with an average RMSD of less than 3 Å, remain relatively stable throughout the MD simulation [62]. Similarly, it was discovered in a study that the ligand and protein RMSD remained between 1.125 and 2.25 Å, indicating that the conformations attained from MDS were structurally stable and ideal for further in silico assessment. These findings are consistent with those of the current study, proving that ZINC72163401, ZINC72358537, and ZINC72358557 form stable complexes with PfHsp90.

Further RMSF and hydrogen bonds analysis confirmed the stability of the complexes formed between ZINC72163401, ZINC72358557, and ZINC72358537 with PfHsp90. The fluctuations were within RMSF

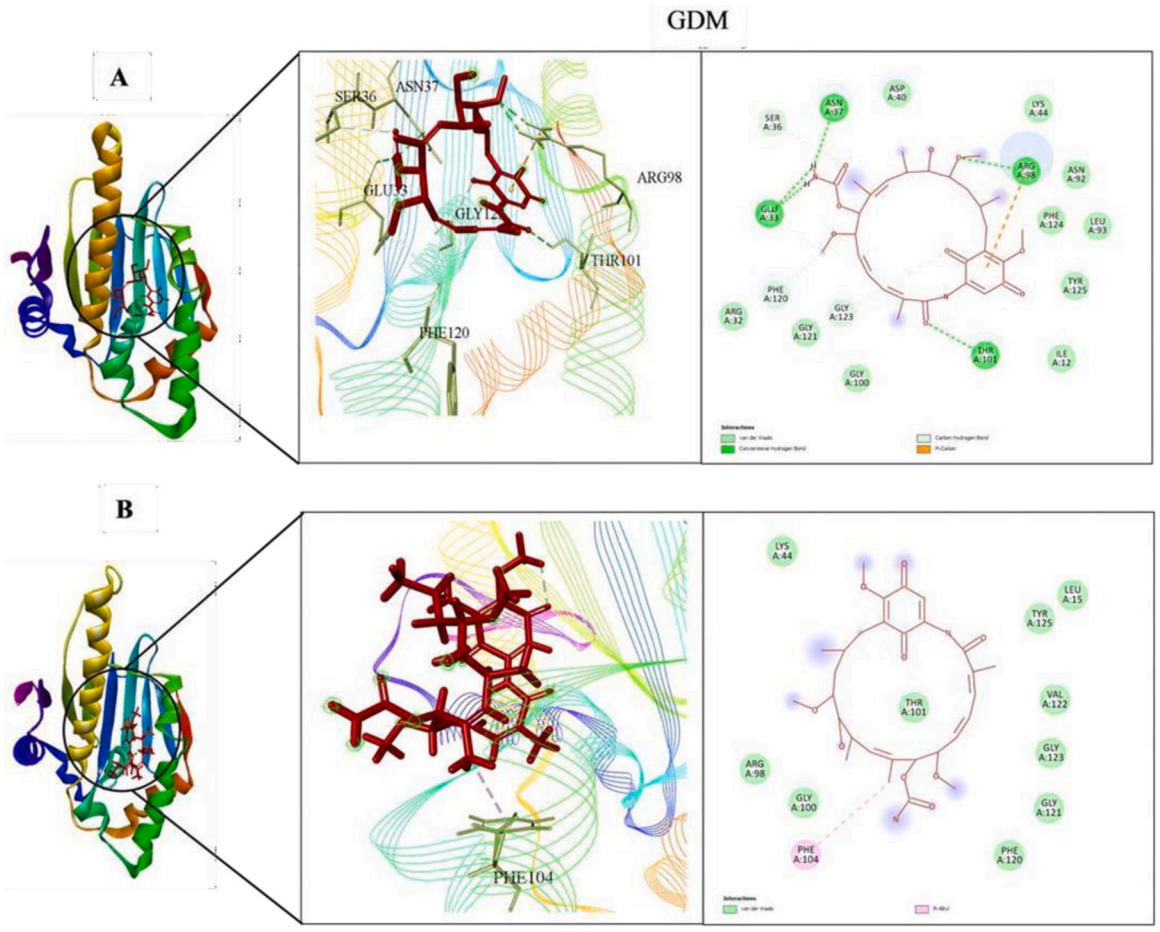


**Fig. 10.** (*continued*).

values of 0.2 nm, which is acceptable when compared with the RMSF value of the reference ligand (GDM). There were no major fluctuations to indicate that the inhibitors' atoms shifted from their average positions during the 100 ns simulation (Fig. 12). This finding is consistent with other studies that ensured RMSF values of their protein–ligand complexes were within acceptable levels to infer their stability [62].

The hydrogen bond analyses (Fig. 13) demonstrated that the potential PfHsp90 inhibitors maintained stable conformation in PfHsp90's active site during the 100 ns simulation, signifying their inhibitory capability. Hydrogen bond formation between a ligand and target protein is essential for a complex's stability because it increases the binding affinity between the two molecules [62]. Authors of a study discovered that the nine hydrogen bonds between ASP 430 as the acceptor and CSMS00081585868 as the donor increased their binding affinity and inhibitory potential [62]. This finding suggests that ZINC09060002, ZINC72163401, and ZINC72358537, which form a maximum of four hydrogen bonds with PfHsp90, and ZINC72358557, which forms six (all higher than the three hydrogen bonds formed between PfHsp90 and GDM), were bound more tightly to the target protein and might possess a better inhibitory capability than GDM.

Since in vitro validation of the inhibitory potential and capability of the lead compounds was also a primary objective of this study, ascertaining their stability in complex with their target proteins was not enough. *In vitro* validation has become a popular approach following MDS in recent drug design and discovery processes [41]. Researchers have performed in vitro validation of the lead compounds they discovered in their respective studies [65–67]. Even though they employed different assays in their studies, they had a common goal that this project shares. The point-to-point calculation found the IC50 values of the three lead compounds to be within 200–400 ng/mL, including that of chloroquine (Fig. 14). These IC50 values can be compared to that of chloroquine to assess their effectiveness levels. Chloroquine was preferred for this comparison because it is utilized to treat susceptible infections with *P. falciparum*, *P. ovale*, *P. vivax*, and *P. malariae*. It is also characterized by low toxicity, an extended duration of action, rapid onset, and high tolerance in humans [68].

According to some studies, the highest concentration of chloroquine utilized for the analysis of chemosensitivity against the 3D strain of *P. falciparum* is 50 nM [69]. Using an online ng/mL to nM calculator (https://savvycalculator.com/ng-mL-to-nm-calculator/ (accessed on 28 March 2024)), the IC50 value of chloroquine was converted to 157 ng/mL. Although chloroquine's IC50 values obtained in this current study (206.47 ng/mL or 66.05 nM) were slightly higher, they were within an acceptable range if the study by Rebelo et al. is anything to go by [70]. In their study, the researchers discovered that in 70 % of their samples, the IC50 values surpassed 200 nM [70]. The authors argued that the high IC50 values could be due to the presence of chloroquine-resistant parasites. However, in this study, the IC50 values of all the PfHsp90 inhibitors were below 150 nM. Even though they are slightly high compared to that of chloroquine, and the inhibitors are required in higher concentrations than chloroquine to treat malaria, at those particular high concentrations, these three PfHsp90 inhibitors might still be effective against malaria. Therefore, ZINC72163401, ZINC72358537, and ZINC72358557 can act as antimalarial drugs against *Plasmodium* malaria. However, further structural optimization studies and clinical testing through in vivo approaches should be performed to ascertain the efficacy of PfHsp90 inhibitors as antimalarial drugs.

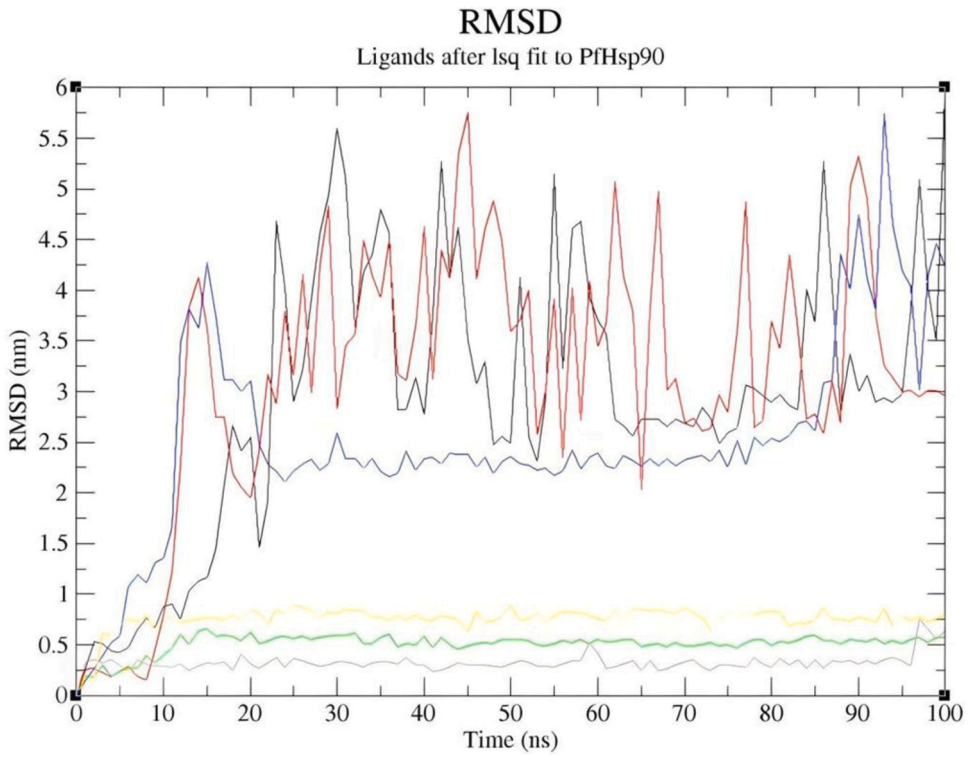


**Fig. 11.** RMSD plot of PfHsp90. (PDB ID: 3K60) with GDM as reference ligand and top-five ZINC database compounds as a function of 100 ns simulation time. ZINC09060002 (Black), ZINC72133064 (red), ZINC72163401 (green), ZINC72358537 (blue), ZINC72358557 (yellow), and GDM (brown).

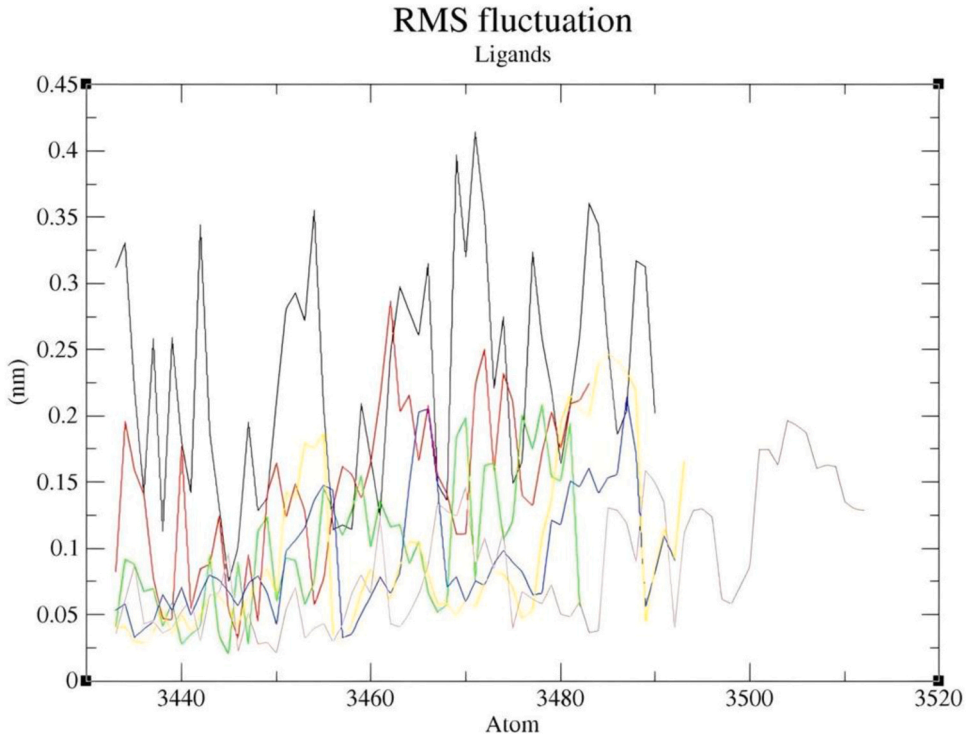


**Fig. 12.** RMSF plot of GDM as reference ligand and top-five ZINC20 database compounds. ZINC09060002 (black), ZINC72133064 (red), ZINC72163401 (green), ZINC72358537 (blue), ZINC72358557 (yellow), and GDM (brown).

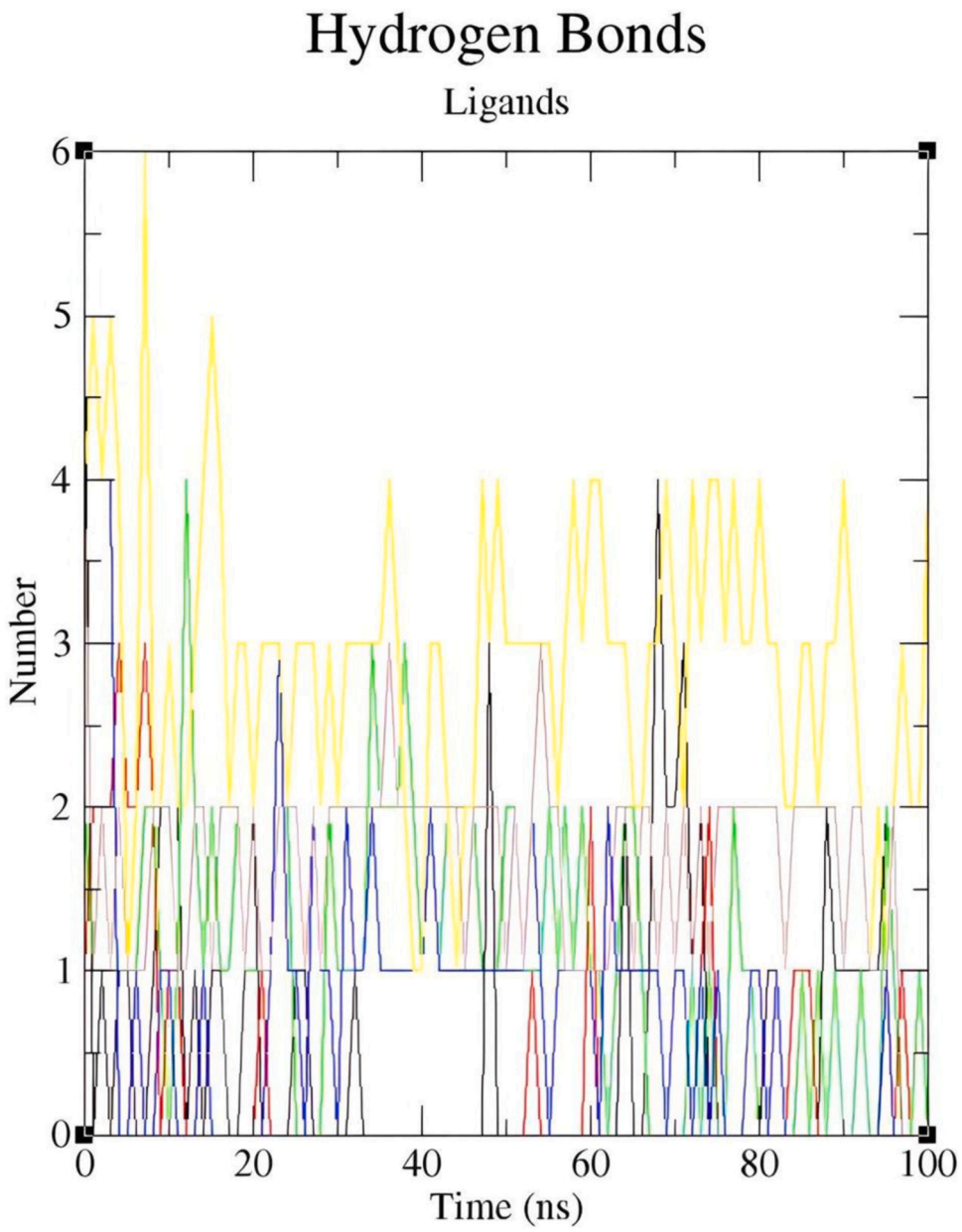


**Fig. 13.** Number of hydrogen bonds plot. The number of hydrogen bonds between PfHsp90 (PDB ID: 3K60) with GDM as reference ligand and top-five ZINC20 database compounds as a function of 100 ns simulation time. ZINC09060002 (black), ZINC72133064 (red), ZINC72163401 (green), ZINC72358537 (blue), ZINC72358557 (yellow), and GDM (brown).

## 4. Materials and methods

### *4.1. Design and software*

A computer-based design was used to find PfHsp90 inhibitors. A computer with the following specifications was used in this research: 11th Gen Intel(R) Core(TM) i7–11800H @ 2.30 GHz. Software such as BIOVIA Discovery Studio (BDS) 2021, PYRX version 0.8, and GROMACS were downloaded and installed into the computer. Web-based servers and databases such as PDB, PubChem, and SwissADME were also used.

### *4.2. PfHsp90 structure retrieval and preparation*

The 3D structure of PfHsp90 was retrieved from PDB database (https://www.rcsb.org/ (accessed on 12 September 2023)). PfHsp90's domain of interest (NTD) was retrieved using PDB ID 3K60 and downloaded in the PDB format. This 3D structure was essential during molecular docking. It was prepared for docking after retrieval using BDS 2021. All bound ligands were removed. Similarly, all heteroatoms, side chains, and water molecules that were far from the binding site and had no influence on the ligand binding were removed as well. These compounds were removed because they do not participate in the interaction between the ligands of interest and PfHsp90. Deleting them presents a desirable pose search and eases computations that would otherwise prove challenging if such compounds clouded the target protein's binding pocket. Another preparation step involved adding polar hydrogens to aid in locating hydrogen bond interactions in the 3D structure. The hydrogen bond interactions are essential to ascertain the ligands' binding affinity to PfHsp90. The prepared 3D structure of PfHsp90 was saved as a.pdb file.

### *4.3. Retrieval of geldanamycin (GDM) structures*

The PubChem library database (https://pubchem.ncbi.nlm.nih.gov/

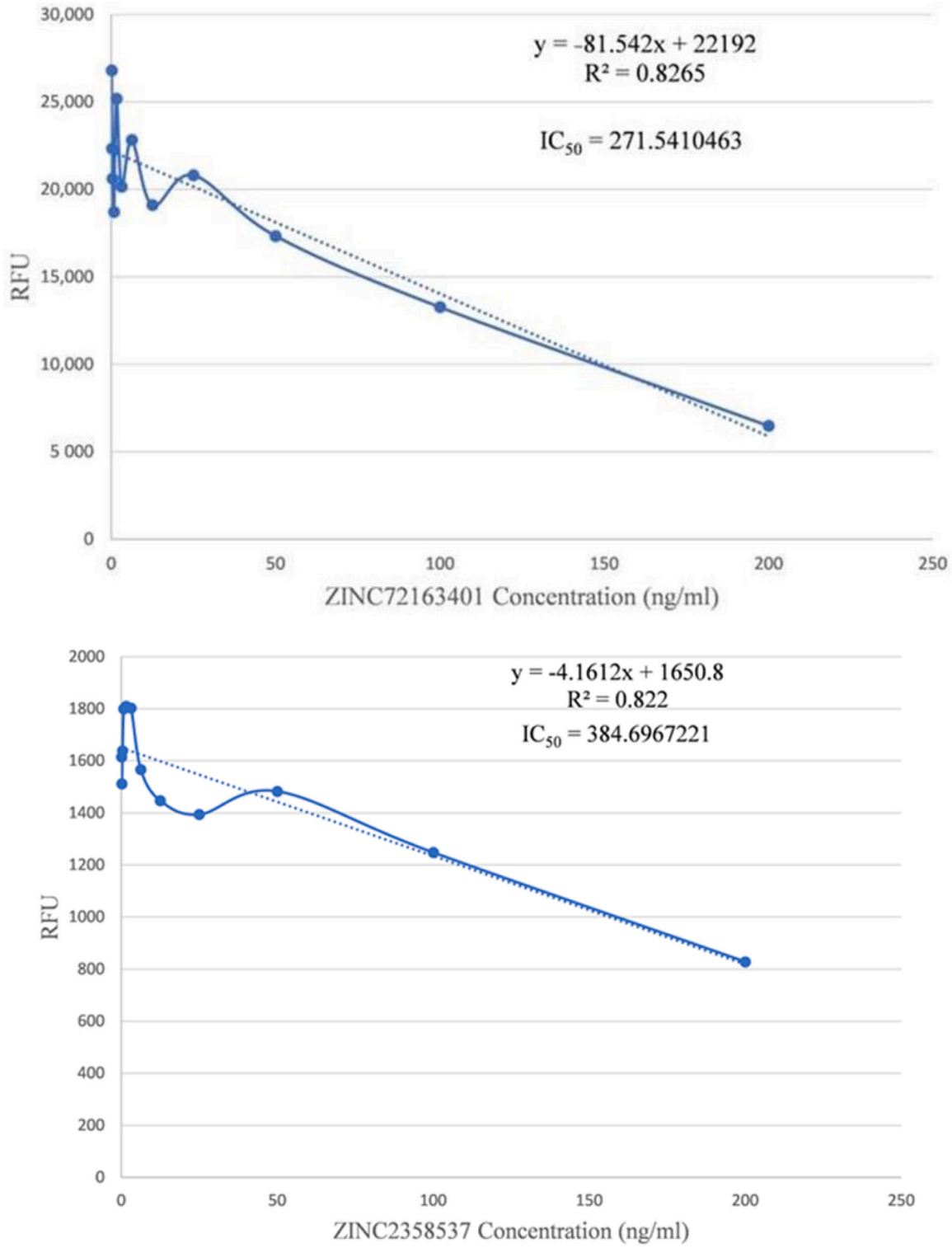


**Fig. 14.** Point-to-point plot. IC50 value determination of PfHsp90 inhibitors and Chloroquine using point-to-point calculation.

(accessed on 12 September 2023)) was used to retrieve the 2D and 3D structures of GDM, an inhibitor of interest. The 3D structure of the ligand will be crucial during virtual screening to classify structurally similar compounds with antimalarial properties or activities.

### *4.4. Pharmacophore-based virtual screening*

The 3D structure of GDM was used to locate active compounds with similar structures that can inhibit PfHsp9. The ZINCPHARMER web server (http://zincpharmer.csb.pitt.edu/pharmer.html (accessed on 13 September 2023)) was used in the process. These active compounds were subjected to further processes to ascertain whether or not they can

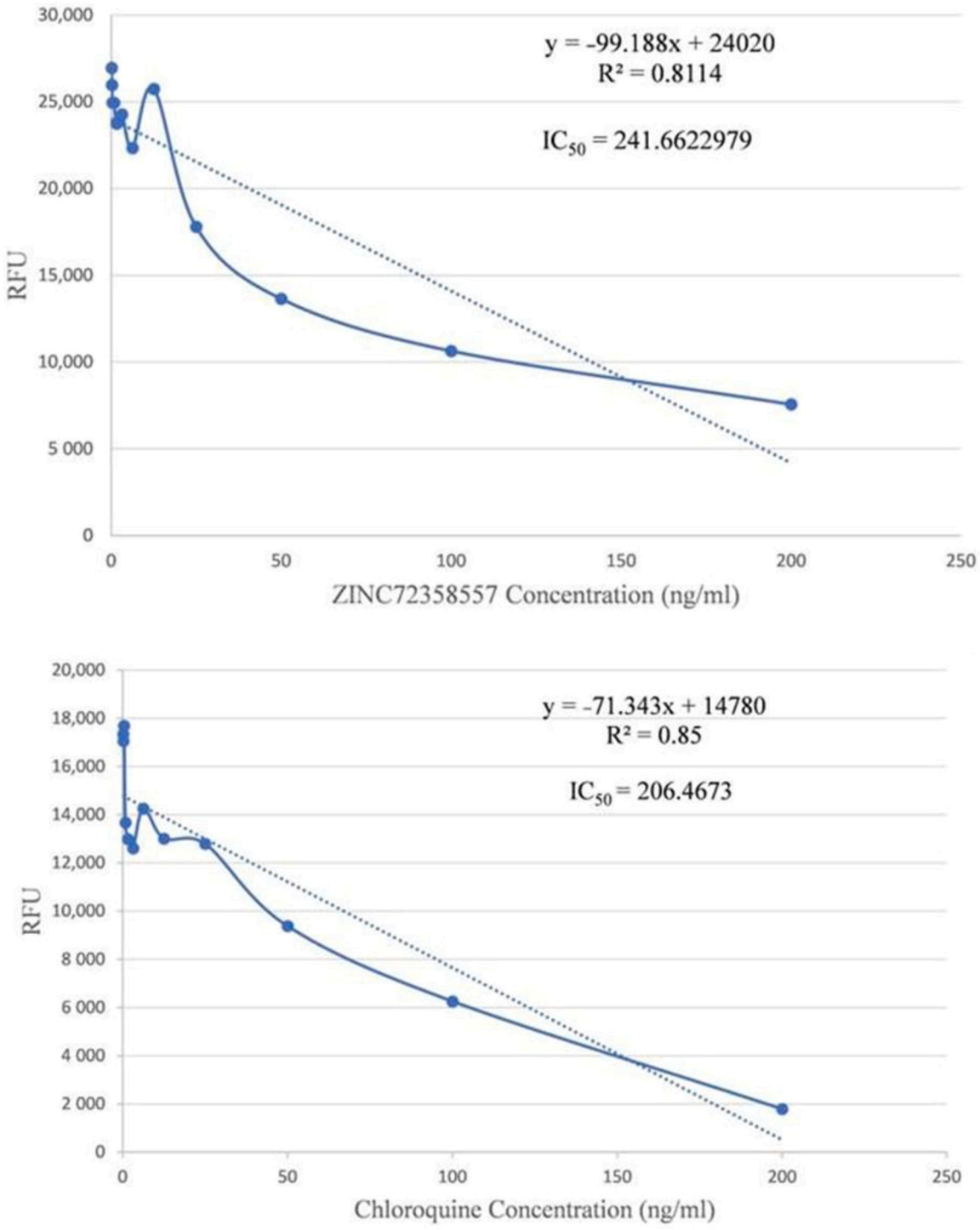


**Fig. 14.** (*continued*).

be used as antimalarial compounds or drugs.

### 4.5. Drug-likeness and pharmacokinetics test

The compounds retrieved from the virtual screening process were subjected to a drug-likeness test to determine their drug like properties and pharmacokinetics analysis to determine their oral bioavailability. SwissADME web tool (http://www.swissadme.ch/ (accessed on 22 September 2023)) was used to perform the drug-likeness test and pharmacokinetics analysis. The SMILES of the virtual screening hits was copy and pasted into the SwissADME web server. The various drug-likeness filters that were utilized include Muegge, Egan, Veber, Ghose, and Lipinski's Rule. These filters assisted in selecting the compounds with desirable drug properties. Similarly, pharmacokinetic results were analyzed in the form of bioavailability radars and the Brain Or IntestinaL EstimateD permeation (BOILED-Egg) diagram. The molecules that satisfied all the bioavailability and permeation and at least four drug-likeness filters' requirements were selected for docking studies.

### 4.6. Molecular docking

The PyRx software version 0.8 was utilized to dock the selected

molecules, potential PfHsp90 inhibitors, with PfHsp90 using Autodock Vina. The format of PfHsp90 was converted from.pdb to.pdbqt using the PyRx software version 0.8. The.pdbqt format is the desirable molecular docking format. The chosen ligand compounds were prepared for molecular docking by minimizing their energies and converting them to a. pdbqt format using the PyRx software version 0.8. The x, y, and z coordinates of the grid that was utilized during docking were 74.1885, –26.0034, and 14.4805, respectively. The grid dimensions were 45.5880 Å (x), 43.8652 Å (y), and 48.7045 Å (z), and the default exhaustiveness value for AutoDock Vina, which is 8, was retained. Molecular docking was then performed, and all protein–ligand complexes with the lowest binding energies were chosen as the final potential candidate drugs. This molecular docking process was also undertaken using the reference ligand, GDM. From the 10 different PfHsp90-GDM complex poses, the best pose was selected and compared to the crystal structure of GDM to determine the docking method's accuracy and capacity to identify significant interactions. Its binding energy was also compared to those of the final potential drug candidates to ascertain whether or not the selected drug candidates preferentially bind to PfHsp90.

### *4.7. Molecular dynamics simulation (MDS)*

The docked complexes of the final drug candidates and PfHsp90 were subjected to MDS to confirm the docking outcomes and perform an in-depth examination of the behavior of the ligands within the target proteins' binding pocket. GROMACS 2022 was used during the MDS process. The GROMACS MDS files, which included topology files for the ligand and protein, and parameter files for the ligand, were first generated using Charmm 36 Force Field from the CHARMM-GUI web server. The CHARMM-GUI web server's default settings were preferred, including water box size options, which was fit to protein size using a rectangular water box type with an edge distance of 10.0. Eighty-five K+ and eighty-one Cl- ions were added to the protein-ligand complexes using Monte Carlo ion placing method, and system temperature was set at 300.00 K. During the GROMACS energy minimization process, the number of steps was set at 5000. The minimized system was equilibrated via a 100 ps run. The final MDS run was set at 100 ns. After the last run, the number of hydrogen bonds, root-mean-square fluctuation (RMSF), and root-mean-square deviation (RMSD) were calculated using GROMACS.

### *4.8. In vitro validation of PfHsp90 inhibitors*

The final PfHsp90 inhibitors were purchased (analytical grade, ≥98 % purity) and subjected to an in vitro validation to ascertain their inhibitory capability without further purification and identity verification. Their antimalarial activity was measured using the SYBR green assay. The inhibitors were dissolved in 300 ul Dimethyl Sulfoxide (DMSO) to a 200 ng/mL concentration. This initial concentration was then serially diluted to 11 dilutions across a 96-well plate (12 columns by 8 rows) using a specific growth media for *Plasmodium* parasites whose preparation is described in WWARN procedure INV02 [71]. A total of 150 µL of each dilution was then pipetted into another plate. Then, 150 µL of a 1 % parasitemic sample was added to each well across the drug coated plate. The dosed plate with parasites was then incubated in a closed system at 37 °C for 3 days, then removed from the incubator and 150 µL lysis buffer containing a DNA intercalating dye (SYBR green 1) added to the wells. The plate was then incubated at room temperature. Thereafter, the Tecan machine was used to read the fluorescence/absorption from surviving parasites. Wavelength readings from this assay were used to describe the inhibition concentration 50 (IC50). Microsoft Excel was used for analysis, translating the figures read from the Tecan machine to a graph. The R2 value generated was a significant value in interpreting the graphs. An R2 value closer to 1 suggests that the regression line is a perfect fit for the data and can be used to calculate the IC50 values.

## 5. Conclusions

The high mortality and morbidity rates caused by malaria necessitate the design and development of new antimalarial medicines. In this study, a thorough in silico drug discovery pipeline to discover PfHsp90 inhibitors was developed. Virtual screening for small molecules using both pharmacophore approaches and docking that identified only five potential PfHsp90 inhibitors was performed. After a molecular dynamics simulation, three potent PfHsp90 inhibitors, ZINC72163401, ZINC72358537, and ZINC72358557, with good activities against *P. falciparum* parasites, were identified. The three potential antimalarial drugs were subjected to in vitro validation using the SYBR Green assay. They exhibited potent inhibitory activity against *P. falciparum* with IC50 values ranging between 200 and 400 ng/mL. The effective antimalarial action and low cytotoxicity of these inhibitors mainly suggested that they may be considered for further structural optimization studies and successive clinical validations. This study offers a valuable in silico blueprint for the rational discovery of novel PfHsp90 inhibitors for *Plasmodium falciparum* malaria treatment.

## Funding

This research received no external funding.

## CRediT authorship contribution statement

**Harrison Onyango:** Writing – original draft, Visualization, Validation, Software, Project administration, Methodology, Investigation, Formal analysis, Data curation, Conceptualization. **Grace Gitau:** Writing – review & editing, Software, Resources. **John Muoma:** Writing – review & editing, Supervision, Software, Resources. **Patrick Okoth:** Writing – review & editing, Validation, Supervision, Software, Resources, Project administration, Conceptualization.

## Declaration of Competing Interest

The authors declare no conflicts of interest; they have no financial or personal relationships that may have inappropriately influenced the writing of this article.

## Acknowledgments

The authors of this manuscript would like to extend their appreciation to Professor Solomon Igosangwa Shibairo, Vice Chancellor (VC) of Masinde Muliro University of Science and Technology (MMUST), and Professor Charles Mutai, Deputy Vice Chancellor (DVC) of Planning Research and Innovation (PRI) at MMUST, for their innovation support (FY22/2023-URF-004), which inspired the writing of this manuscript. Additionally, we thank Professor Hussein S. A. Golicha, Deputy Vice Chancellor (DVC) of Academics and Students Affairs (ASA) at MMUST, for creating a conducive environment for students to perform research and prepare such manuscripts.

### *Author Contributions*

H.O., G.G., P.O., and J.M. conceptualized the study. H.O. collected data, analyzed, and drafted the original manuscript. G.G., P.O., and J.M. offered the much-required technical support. P.O. supervised the project and gave technical expert advice. All authors have read and agreed to the published version of the manuscript.

### *Institutional Review Board Statement*

Not applicable.

*Informed Consent Statement*

Not applicable.

## Appendix A. Supporting information

Supplementary data associated with this article can be found in the online version at doi:10.1016/j.csbr.2024.100018.

## References


[1] WHO. Malaria. World Health Organization. 2022. Available online: https://www.who.int/news-room/fact-sheets/detail/malaria (accessed on 7 August 2022).

[2] WHO. World malaria report 2020. World Health Organization. 2020. Available online: https://www.who.int/teams/global-malaria-programme/reports/world-malaria-report-2020 (accessed on 9 September 2024).

[3] Oladipo HJ, Tajudeen YA, Oladunjoye IO, Yusuff SI, Yusuf RO, Oluwaseyi EM, et al. Increasing challenges of malaria control in sub-Saharan Africa: priorities for public health research and policy-makers. Ann Med Surg 2022;81:104366. https://doi.org/10.1016/j.amsu.2022.104366.

[4] Sá M, Costa DM, Tavares J. Imaging infection by vector-borne protozoan parasites using whole-mouse bioluminescence. Bioluminescence. Methods in Molecular Biology, Vol. 2524. Humana: New York, NY, USA,; 2022. p. 353–66. https://doi.org/10.1007/978-1-0716-2453-1_29.

[5] Ramos, S.; Ademolue, T.W.; Jentho, E.; Wu, Q.; Guerra, J.; Martins, R.; Pires, G.; Weis, S.; Carlos, A.R.; Mahú, I.; et al. A hypometabolic defense strategy against plasmodium infection. BioRxiv 2021, 34, 1–62. https://doi.org/10.1101/2021.09.08.459402.

[6] Laurens MB. RTS, S/AS01 vaccine (Mosquirix™): an overview. Hum Vaccin Immunother 2020;16:480–9. https://doi.org/10.1080/21645515.2019.1669415.

[7] Nadeem AY, Shehzad A, Islam SU, Al-Suhaimi EA, Lee YS. Mosquirix™ RTS, S/AS01 vaccine development, immunogenicity, and efficacy. Vaccines 2022;10:713. https://doi.org/10.3390/vaccines10050713.

[8] C.D.C.About malaria. Center for disease control and prevention. 2022. Available online: ⟨https://www.cdc.gov/malaria/about/faqs.html#:~:text=Symptoms%20of%20malaria%20include%20fever,loss%20of%20red%20blood%20cells⟩ (accessed on 7 August 2022).

[9] Ayanful-Torgby R, Quashie NB, Boampong JN, Williamson KC, Amoah LE. Seasonal variations in Plasmodium falciparum parasite prevalence assessed by varying diagnostic tests in asymptomatic children in southern Ghana. PLOS One 2018;13:e0199172. https://doi.org/10.1371/journal.pone.0199172.

[10] Chew M, Ye W, Omelianczyk RI, Pasaje CF, Hoo R, Chen Q, et al. Selective expression of variant surface antigens enables Plasmodium falciparum to evade immune clearance in vivo. Nat Commun 2022;13:4067. https://doi.org/10.1038/s41467-022-31741-2.

[11] Gross M. Fresh efforts needed against malaria. Curr Biol 2019;29:R301–3. https://doi.org/10.1016/j.cub.2019.04.041.

[12] Wang LT, Pereira LS, Flores-Garcia Y, O'connor J, Flynn BJ, Schön A, et al. A potent anti-malarial human monoclonal antibody targets circumsporozoite protein minor repeats and neutralizes sporozoites in the liver. Immunity 2020;53:733–44. https://doi.org/10.1016/j.immuni.2020.08.014.

[13] C.D.C.. Drug Resistance in the Malaria-Endemic World. Center for Disease Control and Prevention. 2018. Available online: https://www.cdc.gov/malaria/malaria_worldwide/reduction/drug_resistance.html (accessed on 7 August 2022).

[14] Maiga FO, Wele M, Toure SM, Keita M, Tangara CO, Refeld RR, et al. Artemisinin-based combination therapy for uncomplicated Plasmodium falciparum malaria in Mali: a systematic review and meta-analysis. Malar J 2021;20:356. https://doi.org/10.1186/s12936-021-03890-0.

[15] Pousibet-Puerto J, Salas-Coronas J, Sánchez-Crespo A, Molina-Arrebola MA, Soriano-Pérez MJ, Giménez-López MJ, et al. Impact of using artemisinin-based combination therapy (ACT) in the treatment of uncomplicated malaria from Plasmodium falciparum in a non-endemic zone. Malar J 2016;15:339. https://doi.org/10.1186/s12936-016-1408-1.

[16] Stoberg ML, Caillet C, de Villiers M, Zininga T. Inhibitors of the plasmodium falciparum Hsp90 towards selective antimalarial drug design: the past, present and future. Cells 2021;10:2849. https://doi.org/10.3390/cells10112849.

[17] Tintó-Font E, Michel-Todó L, Russell TJ, Casas-Vila N, Conway DJ, Bozdech Z, et al. A heat-shock response regulated by the PfAP2-HS transcription factor protects human malaria parasites from febrile temperatures. Nat Microbiol 2021;6:1163–74. https://doi.org/10.1038/s41564-021-00940-w.

[18] Zininga T, Makumire S, Gitau GW, Njunge JM, Pooe OJ, Klimek H, et al. Plasmodium falciparum Hop (PfHop) interacts with the Hsp70 chaperone in a nucleotide-dependent fashion and exhibits ligand selectivity. PLOS One 2015;10:e0135326. https://doi.org/10.1371/journal.pone.0135326.

[19] Chakrabarti A, Singh V, Singh S. Management and control of antimalarial drug resistance. In: Mandal S, Paul D, editors. Bacterial Adaptation to Co-resistance. Singapore: Springer; 2019. https://doi.org/10.1007/978-981-13-8503-2_15.

[20] Spiegelberg D, Abramenkovs A, Mortensen ACL, Lundsten S, Nestor M, Stenerlöw B. The HSP90 inhibitor Onalespib exerts synergistic anti-cancer effects when combined with radiotherapy: an in vitro and in vivo approach. Sci Rep 2020;10:5923. https://doi.org/10.1038/s41598-020-62293-4.

[21] Honoré FA, Méjean V, Genest O. Hsp90 is essential under heat stress in the bacterium Shewanella oneidensis. Cell Rep 2017;19:680–7. https://doi.org/10.1016/j.celrep.2017.03.082.

[22] Schopf FH, Biebl MM, Buchner J. The HSP90 chaperone machinery. Nat Rev Mol Cell Biol 2017;18:345–60. https://doi.org/10.1038/nrm.2017.20.

[23] Mader, S.L.; Lopez, A.; Lawatscheck, J.; Luo, Q..; Rud, D.A.; Gamiz-Hernandez, A. P.; Sattler, M.; Buchner, J.; Kaila, V.R.I. Conformational dynamics modulate the catalytic activity of the molecular chaperone Hsp90. Nat. Commun. 2020, 11, 1410. https://doi.org/10.1038/s41467–020-15050–0.

[24] Li L, Wang L, You QD, Xu XL. Heat shock protein 90 inhibitors: an update on achievements, challenges, and future directions. J Med Chem 2019;63:1798–822. https://doi.org/10.1021/acs.jmedchem.9b00940.

[25] Silva NS, Torricillas MS, Minari K, Barbosa LR, Seraphim TV, Borges JC. Solution structure of plasmodium falciparum Hsp90 indicates a high flexible dimer. Arch Biochem Biophys 2020;690:108468. https://doi.org/10.1016/j.abb.2020.108468.

[26] Radli M, Rüdiger SG. Dancing with the diva: Hsp90–client interactions. J Mol Biol 2018;430:3029–40. https://doi.org/10.1016/j.jmb.2018.05.026.

[27] Rashid S, Lee BL, Wajda B, Spyracopoulos L. Nucleotide binding and active site gate dynamics for the Hsp90 chaperone ATPase domain from benchtop and high field $^{19}$F NMR spectroscopy. J Phys Chem B 2020;124:2984–93. https://doi.org/10.1021/acs.jpcb.0c00626.

[28] Koren J, Blagg BS. The right tool for the job: an overview of Hsp90 inhibitors. HSF1 and Molecular Chaperones in Biology and Cancer. Cham, Swiderland: Springer,; 2020. p. 135–46. https://doi.org/10.1007/978-3-030-40204-4_9.

[29] Han J, Goldstein LA, Hou W, Chatterjee S, Burns TF, Rabinowich H. HSP90 inhibition targets autophagy and induces a CASP9-dependent resistance mechanism in NSCLC. Autophagy 2018;14:958–71. https://doi.org/10.1080/15548627.2018.1434471.

[30] Whitesell L, Robbins N, Huang DS, McLellan CA, Shekhar-Guturja T, LeBlanc EV, et al. Structural basis for species-selective targeting of Hsp90 in a pathogenic fungus. Nat Commun 2019;10:402. https://doi.org/10.1038/s41467-018-08248-w.

[31] Mak OW, Sharma N, Reynisson J, Leung IK. Discovery of novel Hsp90 C-terminal domain inhibitors that disrupt co-chaperone binding. Bioorg Med Chem Lett 2021;38:127857. https://doi.org/10.1016/j.bmcl.2021.127857.

[32] Park H-K, Yoon NG, Lee J-E, Hu S, Yoon S, Kim SY, et al. Unleashing the full potential of Hsp90 inhibitors as cancer therapeutics through simultaneous inactivation of Hsp90, Grp94, and TRAP1. Exp Mol Med 2020;52:79–91. https://doi.org/10.1038/s12276-019-0360-x.

[33] Huck JD, Que NL, Immormino RM, Shrestha L, Taldone T, Chiosis G, et al. NECA derivatives exploit the paralog-specific properties of the site 3 side pocket of Grp94, the endoplasmic reticulum Hsp90. J Biol Chem 2019;294:16010–9. https://doi.org/10.1074/jbc.RA119.009960.

[34] Que NL, Crowley VM, Duerfeldt AS, Zhao J, Kent CN, Blagg BS, et al. Structure based design of a Grp94-selective inhibitor: Exploiting a key residue in Grp94 to optimize paralog-selective binding. J Med Chem 2018;61:2793–805. https://doi.org/10.1021/acs.jmedchem.7b01608.

[35] Zhang FZ, Ho DHH, Wong RHF. Triptolide, a HSP90 middle domain inhibitor, induces apoptosis in triple manner. Oncotarget 2018;9:22301–15. https://doi.org/10.18632/oncotarget.24737.

[36] Bopp B, Ciglia E, Ould-Chaib A, Groth G, Gohlke H, Jose J. Design and biological testing of peptidic dimerization inhibitors of human Hsp90 that target the C-terminal domain. Biochim Et Biophys Acta (BBA)-Gen Subj 2016;1860:1043–55. https://doi.org/10.1016/j.bbagen.2016.01.005.

[37] Dutta T, Singh H, Edkins AL, Blatch GL. Hsp90 and associated co-chaperones of the malaria parasite. Biomolecules 2022;12:1018. https://doi.org/10.3390/biom12081018.

[38] Posfai D, Eubanks AL, Keim AI, Lu K-Y, Wang GZ, Hughes PF, et al. Identification of Hsp90 inhibitors with anti-Plasmodium activity. Antimicrob Agents Chemother 2018;62:e01799-17. https://doi.org/10.1128/AAC.01799-17.

[39] Wang T, Mäser P, Picard D. Inhibition of Plasmodium falciparum Hsp90contributes to the anti-malarial activities of amino-alcohol-carbazoles. J Med Chem 2016;59:6344–52. https://doi.org/10.1021/acs.jmedchem.6b00591.

[40] Zininga T, Shonhai A. Small molecule inhibitors targeting the heat shock protein system of human obligate protozoan parasites. Int J Mol Sci 2019;20:5930. https://doi.org/10.3390/ijms20235930.

[41] Onyango OH. In silico models for anti-COVID-19 drug discovery: a systematic review. Adv Pharmacol Pharm Sci 2023;2023:4562974. https://doi.org/10.1155/2023/4562974.

[42] Onyango H, Odhiambo P, Angwenyi D, Okoth P. In silico identification of new anti-SARS-CoV-2 main protease (Mpro) molecules with pharmacokinetic properties from natural sources using molecular dynamics (MD) simulations and hierarchical virtual screening. J Trop Med 2022;2022:3697498. https://doi.org/10.1155/2022/3697498.

[43] Mengist HM, Dilnessa T, Jin T. Structural basis of potential inhibitors targeting SARS-CoV-2 main protease. Front Chem 2021;9:622898. https://doi.org/10.3389/fchem.2021.622898.

[44] Tahghighi A, Mohamadi-Zarch SM, Rahimi H, Marashiyan M, Maleki-Ravasan N, Eslamifar A. In silico and in vivo antimalarial investigation on 1-(heteroaryl)-2-((5-nitroheteroaryl) methylene) hydrazine derivatives. Malar J 2020;19:231.

[45] Sachdeva C, Wadhwa A, Kumari A, Hussain F, Jha P, Kaushik NK. In silico potential of approved antimalarial drugs for repurposing against COVID-19. Omics A J Integr Biol 2020;24:568–80.

[46] Sinha S, Sarma P, Sehgal R, Medhi B. Development in assay methods for in vitro antimalarial drug efficacy testing: a systematic review. Front Pharmacol 2017;8:754. https://doi.org/10.3389/fphar.2017.00754.

[47] Cheruiyot, A.C.; Auschwid, J.M.; Lee, P.J.; Yeda, R.A.; Okello, C.O.; Leed, S.E.; Talwar, M.; Murthy, T.; Gaona, H.W.; et al. Hickman, M.R. Assessment of the Worldwide antimalarial resistance network standardized procedure for in vitro malaria drug sensitivity testing using SYBR green assay for field samples with various initial parasitemia levels. Antimicrob. Agents Chemother. 2016, 60, 2417–2424. https://doi.org/10.1128/AAC.00527–15.
[48] K. Traoré S.A. Diakité S. Bah D.S. Konaté D. Dabitao I. Sanogo M. Sangaré S. Dama B. Keita M. Doumbouya. et al. Susceptibility of Plasmodium falciparum isolates to antimalarial drugs in a highly seasonal malaria endemic village in Mali. 2019, preprint. https://doi.org/10.21203/rs.2.17605/v1.
[49] Duan M, Bai Y, Deng S, Ruan Y, Zeng W, Li X, et al. Different in vitro drug susceptibility profile of plasmodium falciparum isolates from two adjacent areas of northeast myanmar and molecular markers for drug resistance. Trop Med Infect Dis 2022;7:442. https://doi.org/10.3390/tropicalmed7120442.
[50] Martínez L. Automatic identification of mobile and rigid substructures in molecular dynamics simulations and fractional structural fluctuation analysis. PLOS One 2015;10:e0119264. https://doi.org/10.1371/journal.pone.0119264.
[51] Su, X.Z.; Lane, K.D.; Xia, L..; Sá, J.M.; Wellems, T.E. Plasmodium genomics and genetics: New insights into malaria pathogenesis, drug resistance, epidemiology, and evolution. Clin. Microbiol. Rev. 2019, 32, 1–29. https://doi.org/10.1128/cmr.00019–19.
[52] Varo R, Chaccour C, Bassat Q. Update on malaria. Med Clín 2020;155:395–402. https://doi.org/10.1016/j.medcli.2020.05.010.
[53] Ashton TD, Devine SM, Möhrle JJ, Laleu B, Burrows JN, Charman SA, et al. The development process for discovery and clinical advancement of modern antimalarials. J Med Chem 2019;62:10526–62. https://doi.org/10.1021/acs.jmedchem.9b00761.
[54] White J, Dhingra SK, Deng X, El Mazouni F, Lee MCS, Afanador GA, et al. Identification and mechanistic understanding of dihydroorotate dehydrogenase point mutations in Plasmodium falciparum that confer in vitro resistance to the clinical candidate DSM265. ACS Infect Dis 2018;5:90–101. https://doi.org/10.1021/acsinfecdis.8b00211.
[55] Alzain AA, Ahmed ZAM, Mahadi MA, Elbadwi FA. Identification of novel Plasmodium falciparum dihydroorotate dehydrogenase inhibitors for malaria using in silico studies. Sci Afr 2022;16:e01214. https://doi.org/10.1016/j.sciaf.2022.e01214.
[56] Murphy SC, Duke ER, Shipman KJ, Jensen RL, Fong Y, Ferguson S, et al. A randomized trial evaluating the prophylactic activity of DSM265 against pre-erythrocytic Plasmodium falciparum infection during controlled human malarial infection by mosquito bites and direct venous inoculation. J Infect Dis 2018;217:693–702. https://doi.org/10.1093/infdis/jix613.
[57] Phillips MA, Lotharius J, Marsh K, White J, Dayan A, White KL, et al. A long-duration dihydroorotate dehydrogenase inhibitor (DSM265) for prevention and treatment of malaria. Sci Transl Med 2015;7:296ra111. https://doi.org/10.1126/scitranslmed.aaa6645.
[58] Sulyok M, Rückle T, Roth A, Mürbeth RE, Chalon S, Kerr N, et al. DSM265 for Plasmodium falciparum chemoprophylaxis: a randomised, double blinded, phase 1 trial with controlled human malaria infection. Lancet Infect Dis 2017;17:636–44. https://doi.org/10.1016/S1473-3099(17)30139-1.
[59] Corbett KD, Berger JM. Structure of the ATP-binding domain of Plasmodium falciparum Hsp90. Proteins Struct Funct Bioinform 2010;78:2738–44. https://doi.org/10.1002/prot.22799.
[60] Onyango OH, Mwenda CM, Gitau G, Muoma J, Okoth P. In-silico analysis of potent Mosquirix vaccine adjuvant leads. J Genet Eng Biotechnol 2023;21:155. https://doi.org/10.1186/s43141-023-00590-x.
[61] Rampogu S, Parate S, Parameswaran S, Park C, Baek A, Son M, et al. Natural compounds as potential Hsp90 inhibitors for breast cancer-Pharmacophore guided molecular modelling studies. Comput Biol Chem 2019;83:107113. https://doi.org/10.1016/j.compbiolchem.2019.107113.
[62] Oduselu GO, Afolabi R, Ademuwagun I, Vaughan A, Adebiyi E. Structure-based pharmacophore modeling, virtual screening, and molecular dynamics simulation studies for identification of Plasmodium falciparum 5-aminolevulinate synthase inhibitors. Front Med 2023;9:1022429.
[63] Gao M, Kang D, Liu N, Liu Y. In silico discovery of small-molecule inhibitors targeting SARS-CoV-2 main protease. Molecules 2023;28:5320. https://doi.org/10.3390/molecules28145320.
[64] Zheng L, Meng J, Jiang K, Lan H, Wang Z, Lin M, et al. Improving protein–ligand docking and screening accuracies by incorporating a scoring function correction term. Brief Bioinform 2022;23:bbac051. https://doi.org/10.1093/bib/bbac051.
[65] Cheng Z, Bhave M, Hwang SS, Rahman T, Chee XW. Identification of potential p38γ inhibitors via in silico screening, In vitro bioassay and molecular dynamics simulation studies. Int J Mol Sci 2023;24:7360. https://doi.org/10.3390/ijms24087360.
[66] Kant V, Kumar P, Ranjan R, Kumar P, Mandal D, Vijayakumar S. In silico screening, molecular dynamic simulations, and in vitro activity of selected natural compounds as an inhibitor of Leishmania donovani 3-mercaptopyruvate sulfurtransferase. Parasitol Res 2022;121:2093–109. https://doi.org/10.1007/s00436-022-07532-5.
[67] Ornnork N, Kiriwan D, Lirdprapamongkol K, Choowongkomon K, Svasti J, Eurtivong C. Molecular dynamics, MM/PBSA and in vitro validation of a novel quinazoline-based EGFR tyrosine kinase inhibitor identified using structure-based in silico screening. J Mol Graph Model 2020;99:107639. https://doi.org/10.1016/j.jmgm.2020.107639.
[68] Zhou W, Wang H, Yang Y, Chen ZS, Zou C, Zhang J. Chloroquine against malaria, cancers and viral diseases. Drug Discov Today 2020;25:2012–22. https://doi.org/10.1016/j.drudis.2020.09.010.
[69] Agarwal P, Anvikar AR, Pillai CR, Srivastava K. In vitro susceptibility of Indian Plasmodium falciparum isolates to different antimalarial drugs & antibiotics. Indian J Med Res 2017;146:622–8. https://doi.org/10.4103/ijmr.IJMR_1688_15.
[70] Rebelo M, Tempera C, Fernandes JF, Grobusch MP, Hänscheid T. Assessing anti-malarial drug effects ex vivo using the haemozoin detection assay. Malar J 2015;14:140. https://doi.org/10.1186/s12936-015-0657-8.
[71] In Vitro Module, WWARN. 2011. Preparation of Complete Medium for Malaria Culture. WWARN Procedure. https://www.iddo.org/sites/default/files/publication/202309/INV02_PreparationOfCompleteMedium.pdf (accessed on 7 August 2023).